Experimental and Computational Analysis of Monkey Smooth Pursuit Eye Movements

Mark M. Churchland and Stephen G. Lisberger

J Neurophysiol 86:741-759, 2001.

Journal of Neurophysiology publishes original articles on the function of the nervous system. It is published 12 times a year (monthly) by the American Physiological Society, 9650 Rockville Pike, Bethesda MD 20814-3991. ISSN: 0022-3077, ESSN: 1522-1598. Visit our website at http://www.the-aps.org/.

Experimental and Computational Analysis of Monkey Smooth Pursuit Eye Movements

MARK M. CHURCHLAND AND STEPHEN G. LISBERGER
Howard Hughes Medical Institute, Department of Physiology, Neuroscience Graduate Program, and W. M. Keck Foundation Center for Integrative Neuroscience, University of California, San Francisco, California 94143

Received 13 October 2000; accepted in final form 3 May 2001

Churchland, Mark M. and Stephen G. Lisberger. Experimental and computational analysis of monkey smooth pursuit eye movements. *J Neurophysiol* 86: 741–759, 2001. Smooth pursuit eye movements are guided by visual feedback and are surprisingly accurate despite the time delay between visual input and motor output. Previous models have reproduced the accuracy of pursuit either by using elaborate visual signals or by adding sources of motor feedback. Our goal was to constrain what types of signals drive pursuit by obtaining data that would discriminate between these two modeling approaches, represented by the "image motion model" and the "tachometer feedback" model. Our first set of experiments probed the visual properties of pursuit with brief square-pulse and sine-wave perturbations of target velocity. Responses to pulse perturbations increased almost linearly with pulse amplitude, while responses to sine wave perturbations showed strong saturation with increasing stimulus amplitude. The response to sine wave perturbations was strongly dependent on the baseline image velocity at the time of the perturbation. Responses were much smaller if baseline image velocity was naturally large, or was artificially increased by superimposing sine waves on pulse perturbations. The image motion model, but not the tachometer feedback model, could reproduce these features of pursuit. We used a revision of the image motion model that was, like the original, sensitive to both image velocity and image acceleration. Due to a saturating nonlinearity, the sensitivity to image acceleration declined with increasing image velocity. Inclusion of this nonlinearity was motivated by our experimental results, was critical in accounting for the responses to perturbations, and provided an explanation for the unexpected stability of pursuit in the presence of perturbations near the resonant frequency. As an emergent property, the revised image motion model was able to reproduce the frequency and damping of oscillations recorded during artificial feedback delays. Our second set of experiments replicated prior recordings of pursuit responses to multiple-cycle sine wave perturbations, presented over a range of frequencies. The image motion model was able to reproduce the responses to sine wave perturbations across all frequencies, while the tachometer feedback model failed at high frequencies. These failures resulted from the absence of image acceleration signals in the tachometer model. We conclude that visual signals related to image acceleration are important in driving pursuit eye movements and that the nonlinearity of these signals provides stability. Smooth pursuit thus illustrates that a plausible neural strategy for combating natural delays in sensory feedback is to employ information about the derivative of the sensory input.

INTRODUCTION

Motor systems rely on sensory feedback. A primary function of feedback is to tell the system how its output differs from the intended output, and to guide corrective movements. In such cases, sensory inputs provide the system with negative feedback. Negative feedback systems have the practical advantage that they are resistant to both noise and miscalibration of internal signals. They also have the drawback that they are prone to instabilities if sensory feedback is not immediate. Sensory processing delays of 100 ms or more are common in the nervous system. How do motor systems maintain good performance in the face of such feedback delays if they rely heavily on a negative feedback architecture?

Smooth pursuit eye movements provide an ideal model system in which to approach this problem. Pursuit has an explicit negative feedback architecture because the source of its sensory inputs, the retina, is attached to the motor effector, the eyeball. As illustrated in Fig. 1, the primary input to the pursuit system is retinal image motion, defined as target motion with respect to the potentially moving eye ($\dot{I} = \dot{T} - \dot{E}$) (Rashbass 1961). The pursuit system is designed to minimize image motion by matching eye velocity to target velocity. The image velocity input to pursuit thus provides both a feedforward signal that drives changes in eye velocity, and a feedback signal regarding the adequacy of those changes. Feedback regarding the effect of motor commands is delayed due the 60- to 130-ms latency between visual input and motor response. Pursuit performance is generally much better than would be expected given this feedback delay. For example, Fig. 2 shows typical pursuit responses to a step-ramp of target position (Rashbass 1961), which delivers a step of target velocity. After a delay of approximately 100 ms, eye velocity increases rapidly, overshoots target velocity little or not at all, and then either oscillates near target velocity with a period of about 200 ms (Fig. 2*B*), or tracks target velocity almost perfectly (Fig. 2*C*).

Models of the pursuit system have been used extensively to form and test hypotheses about how neural systems achieve the performance measured in human and monkey subjects. The simplest pursuit model uses only a single visual input, an image velocity signal, and instantiates the "visual system" box in Fig. 1 as a simple gain. Eye acceleration would then be proportional to image velocity with a delay of 60–130 ms. In the absence of delay, such a "velocity-servo" model performs well, as eye acceleration is always in the direction that reduces image motion. However, in the presence of delay, the velocity

Address for reprint requests: M. M. Churchland, Dept. of Physiology, UCSF, Box 0444, 513 Parnassus Ave., San Francisco, CA 94143-0444 (E-mail: mchurchl@phy.ucsf.edu).

The costs of publication of this article were defrayed in part by the payment of page charges. The article must therefore be hereby marked "*advertisement*" in accordance with 18 U.S.C. Section 1734 solely to indicate this fact.

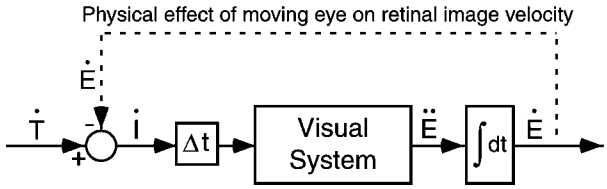

FIG. 1. Schematic diagram of the basic functional organization of the pursuit system. Target velocity ($\dot{T}$) and eye velocity ($\dot{E}$) are compared at the retina to yield image velocity ($\dot{I}$). Image velocity is delayed (Δt) and processed by the visual system to produce a command for eye acceleration ($\ddot{E}$). The eye acceleration command is integrated to produce eye velocity ($\dot{E}$), which we treat as the output of the pursuit system. Solid lines show the flow of neural signals, while the dashed line shows physical negative feedback due to the fact that the retina is attached to the moving eyeball.

servo model performs poorly and fails to account for a number of the features exhibited by pursuit. Figure 2, *B* and *C*, shows typical examples of eye velocity during pursuit, while the performance of the velocity-servo model is illustrated in Fig. 2*D*. The model exhibits much more overshoot than is seen in the data and oscillates with much too low of a frequency.

These failings of the simple velocity-servo model are eliminated, in different ways, by three classes of pursuit model that have been published previously, each of which is able to account for pursuit responses to step changes in target velocity like those shown in Fig. 2, *B* and *C*. However, the three models use different control strategies and make fundamentally different predictions about the organization of the neural circuits that mediate pursuit. Two of these, the "target velocity" model of Robinson (Dicke and Thier 1999; Huebner et al. 1990, 1992; Pola and Wyatt 2001; Robinson et al. 1986) and the "tachometer feedback" model of Ringach (1995), assume that pursuit eye movements are guided by motor feedback signals, and that the visual pathways driving pursuit are sensitive only to image velocity. The third, the "image motion" model of Krauzlis and Lisberger (1989, 1994b) assumes that pursuit is driven not only by image velocity, but also by image acceleration.

Goldreich et al. (1992) have shown that the target velocity model cannot account for the changes in spontaneous oscillation frequency produced by altering the visual feedback delay. We therefore focus on experiments and simulations designed to discriminate between the tachometer feedback and image motion models, and to determine whether the accuracy of pursuit is due to motor feedback or to elaborated visual inputs. Our experiments provide new data that could be reproduced only by a modified version of the image motion model. We conclude that the remarkable accuracy of pursuit in human and nonhuman primates is due to visual inputs related to image velocity and image acceleration. We further conclude that the unexpected stability of pursuit, remarked on under a variety of circumstances (Goldreich et al. 1992; Ringach 1995; Robinson 1965), results from a nonlinearity implied by our data.

METHODS

Experiments on monkeys

The majority of pursuit data shown was collected specifically for this paper. The exception is the data from *monkey Jo* in Fig. 11, which is reprinted from Fig. 3 of Goldreich et al. (1992) and shows responses under conditions of artificially increased feedback delays. These data were included because Ringach (1995) has argued that the image motion model cannot account for them.

Data were obtained from three rhesus monkeys using methods that had been approved in advance by the Committee on Animal Research at UCSF. Using sterile procedure under isoflurane anesthesia, monkeys were implanted with a platform that allowed head restraint and a scleral search coil for monitoring eye movements (Judge et al. 1980). They were given postoperative analgesic doses of Buprenorphine (0.01 mg/kg) every 12 h for 2–3 days. Monkeys were trained to track visual targets for a juice reward. During the experiment, monkeys sat in a primate chair with their head restraint device fixed to the ceiling of the chair. Targets were projected onto the back of a tangent screen that was 114 cm in front of the monkey. A red fixation spot was provided by direct projection of the image from a red light-emitting diode (LED) onto the center of the screen. A 0.5° white moveable tracking target was created by reflecting the beam from an optical bench off a pair of orthogonal mirror galvanometers. The fixation and tracking targets had luminances of 0.2 and 3.5 cd/m^2, respectively. The room was otherwise dark.

Stimuli were presented in individual trials. Daily experiments lasted about 2 h, during which we collected eye movement responses for 1,600 to 3,000 trials. Trials began with the appearance of the red fixation spot, which the monkey was required to fixate. After a

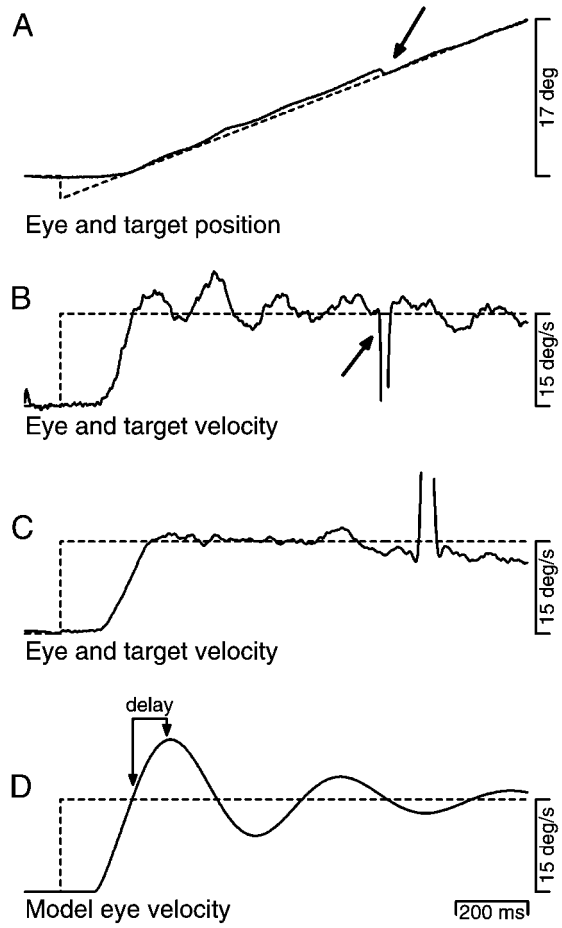

FIG. 2. Representative pursuit responses to step-ramp target motion. *A*: superimposed eye position (—) and target position (- - - - -) from a response of *monkey Na* for a leftward target step of 2° followed by ramp target motion to the right at 15°/s. The diagonal arrow points out a small saccade that occurred near the end of the trial. *B*: eye velocity (—) and target velocity (- - - - -) for the same response as shown in *A*. The diagonal arrow points out the rapid deflection of eye velocity associated with the small leftward saccade. To facilitate viewing, the saccadic eye velocity has been truncated. *C*: eye and target velocity from a response of *monkey Ka* to the same step-ramp target motion. *D*: response obtained by simulating the linear "velocity-servo" model described in the text with a total visual-motor delay of 95 ms.

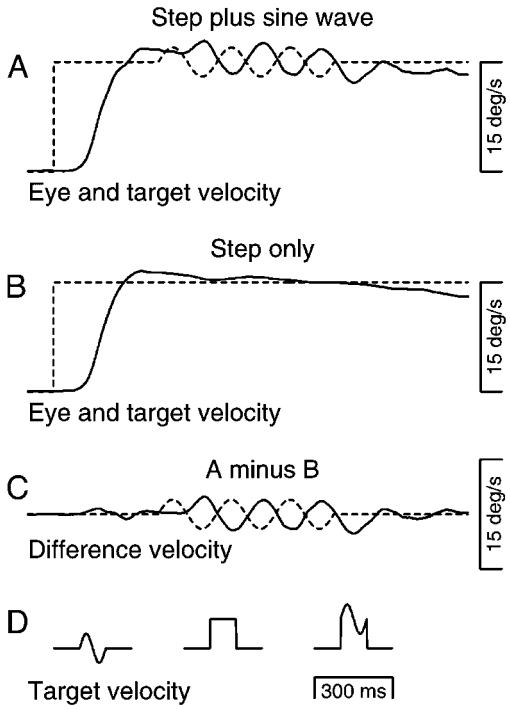

FIG. 3. Methods used to isolate responses to perturbations imposed on ongoing target motion. Solid and dashed traces show average eye velocity and target velocity, respectively. All averages are from *monkey Na* and are triggered on the onset of target motion. *A*: average response to a ±2°/s sinusoidal perturbation of period 225 ms superimposed on a 15°/s velocity step. *B*: average response to the velocity step alone. Spontaneous oscillations are obscured by averaging. *C*: difference eye velocity, obtained by taking the point-by-point difference between the responses in *A* and *B*. *D*: target velocity perturbations used to test open-loop pursuit: a single cycle of a 10-Hz sine wave (*left*), a 100-ms-long pulse of target velocity (*middle*), and the superposition of the pulse and sine wave (*right*).

variable delay of 700–1,100 ms, the fixation spot was extinguished, and the white tracking target appeared 1.5–2.5° to the left or right and began to move immediately. The exact eccentricity was set to reduce the occurrence of saccades and varied depending on the monkey. The target always moved toward and then well past the extinguished fixation point. The target moved for a variable period of at least 1,600 ms. Each monkey was required to track the target with an accuracy of 3° until it was extinguished, at which time he received a reward. Usually, the target moved at a constant velocity of 15°/s. In some trials, perturbations were imposed on the constant target velocity. Perturbations were either sinusoidal variations of target velocity, brief pulses of target velocity, or combinations of pulses and sine waves. The position excursion of the perturbations ranged from 0.06 to 1.2° and was therefore small enough so that their presence did not affect the monkey's ability to keep eye position within the window required for reward. Different trial types were presented in random order, weighted so that perturbations were present in only 25% of the trials.

Eye and target position and eye velocity were sampled at 1 kHz on each channel. The eye velocity voltage was obtained by using an analog circuit that differentiated signals at frequencies up to 25 Hz and attenuated signals at higher frequencies (−20 dB per decade). The target position voltages were obtained as feedback from sensors on the mirror galvanometers. Actual target velocity lagged commanded target velocity by 2 ms or 7.2° at 10 Hz. Analog differentiation of eye position voltages to create the eye velocity signal introduced phase lag that was negligible at low frequencies but corresponded to up to 7 ms of time delay in the frequency range of 8–11 Hz. These lags were corrected in the data analysis.

Saccades were identified by eye, and the resulting deflections of eye velocity were replaced with straight-line segments. For our purposes, the practice of linear interpolation is practically and theoretically preferable to other alternatives, such as treating the excised saccades as missing data (see Churchland and Lisberger 2000), although under our stimulus conditions the two methods produce very similar results. For the majority of our data, saccades were both small and rare, occurring about once per second, although there was day-to-day and monkey-to-monkey variability in the number of saccades. Trials were rejected in the rare (1–5% depending on the experiment) instances when saccades were numerous, indicating that smooth tracking was poor. For experiments in which we examined the response to 100-ms-long perturbations of target velocity, trials were rejected from the analysis if a saccade obscured the response or occurred during the target perturbation. Additionally, after discovering the effect of baseline image velocity on the response to perturbations, for some analyses (Figs. 4 and 5) we rejected trials in which eye velocity was not close to target velocity when the perturbation was imposed. For some experiments, the requirement both that eye velocity be near target velocity at the time of the perturbation, and that no saccade interrupt the target perturbation or obscure the response, caused as many as 40% of trials to be excluded from analysis. Although we considered it important to exclude these trials on principle, their inclusion had only the minor (and expected) effect of making the average responses slightly smaller.

For each trial type, we aligned individual trials on the onset of target motion and computed the average eye velocity evoked by the target. We isolated the pursuit response to perturbations of target velocity (Fig. 3*C*) by computing the millisecond-by-millisecond difference between the average response to target steps that included (Fig. 3*A*) or did not include (Fig. 3*B*) a perturbation. We presented perturbations on top of ongoing target motion because the pursuit system responds well to high-frequency perturbations only after it has already been engaged by some other target motion (Goldreich et al. 1992; Schwartz and Lisberger 1994).

For sinusoidal perturbations, we used the Fourier transform to compute the gain and phase shift of both monkey and model responses. The gain was estimated as the amplitude of the relevant frequency component of the eye velocity response, divided by the amplitude of the target velocity perturbation. The phase shift was estimated as the difference between the phase of the response and that of the target. For perturbations that delivered pulses of image velocity, response amplitude was calculated as the difference between the maximum and minimum eye velocities over a period that began 40 ms before the response and ended at the time of the peak of the response. To remove the small contributions of noise, we subtracted the same measure for trials in which perturbations were not presented. The impact of this correction was minor (<10%).

Computer simulations

Models were simulated on a DEC Alpha workstation using our revision of the ASP software originally written by L. M. Optican and H. P. Goldstein. To allow for greater flexibility in the cost function used during optimizations, some optimizations were run using compiled Matlab functions with gradient descent provided by the "constr" function. Simplified versions of both models, employing an intuitive graphical interface, can be explored with common web browsers at http://keck.ucsf.edu/~sgl/top_pursuitmodel.htm.

Models were built by interconnecting time delays, nonlinearities, and low-pass filters. Optimized parameters were the time delays, the coefficients describing each of the nonlinearities, and the time constants of the low-pass filters, which converted step inputs into exponentially relaxing outputs with a single time constant. Optimization was typically initiated by manually adjusting the model parameters until the responses were reasonably close to those of the monkey. For example, for the fits shown in Figs. 12 and 13, the parameters of both models were initially set so that each provided reasonable approxi-

mations to the 15°/s step responses and produced responses to sinusoidal perturbations that were in the right amplitude range. Optimization employed a gradient descent algorithm ("stepit," Chandler 1965). To speed the optimization process, limits were initially set on the range of most parameters. If a good fit was not achieved within this range, the limits were relaxed or eliminated. When a good fit was achieved, the optimization algorithm typically took little time in finding it. In cases where a good fit was not achieved, we repeatedly restarted the optimization algorithm using different initial parameters. Different initial parameters were obtained by *1*) "jiggling" the parameter values slightly from their value at the error minimum, *2*) setting the parameters to new random values, and *3*) setting the parameters by hand to attempt to improve the fit. The cost function was usually simply the sum of the millisecond by millisecond squared difference between the model and the data. For the simulations in Fig. 10, we included in the cost function the error between measured aspects of the pursuit and model responses (e.g., the response amplitude). When some aspects of the data were fit better than others, we increased the cost function for those traces that were not fit well (multiplying their error by a constant), and continued optimization. This was useful in fitting the model simultaneously to large magnitude responses (e.g., the response to a 15°/s step) and small magnitude responses (e.g., the response to a 10-Hz target). Thus in instances where fits were consistently poor we think it unlikely that we missed the global error minimum. Our confidence in this assertion is increased by the nature of the failures observed in instances of poor fits, which are readily explained by reference to the architecture of the models. Pursuit initiation from fixation is typically 10–20 ms slower than the true pursuit latency. Models were allowed to compensate by having the optimization algorithm add an additional delay at initiation.

RESULTS

Open-loop responses to brief perturbations of target velocity

We begin by presenting the results of experiments designed to test the feed-forward properties of pursuit. We recorded responses to 100-ms-long perturbations consisting of pulses (Fig. 4*A*) or sine wave modulations (Fig. 4*B*) of target velocity. Responses were recorded to various amplitudes of each perturbation type. Figure 4, *A* and *B*, shows averages of eye velocity. The pursuit response to a 12°/s velocity pulse was more than twice as large as the response to a 4°/s pulse, although not quite three times as large. In contrast, the response was nearly the same for a 12°/s sinusoidal perturbation as for a 4°/s perturbation. Note that, for graphical visibility, the eye velocity responses in Fig. 4, *A* and *B*, are plotted at twice the vertical scale as the target velocity traces.

The differing nonlinearity of the responses to pulse and sinusoidal perturbations is summarized for *monkey Na* in Fig. 4*C*, which plots response amplitude as a function of stimulus amplitude. The response to velocity pulse perturbations (□) saturates moderately with stimulus amplitude over the range of 1–12°/s. The response to a 12°/s pulse is 60% as large as expected given a linear extrapolation from the response to a 2°/s pulse. The dashed line shows that a logarithmic fit captures well the small to moderate response saturation. The responses to sinusoidal perturbations saturated much more severely (● and ▲). The saturation was similar whether we measured the response to the first cycle of a perturbation that was five cycles long (●) or the average response to all five cycles (▲). The response to the first cycle of a 12°/s amplitude sine wave is only 33% as large as expected given a linear extrapolation from the response to a 2°/s sine wave. The response to all five cycles is 38% as large as expected given a linear extrapolation. These data were well fit by a logarithmic relationship (solid and finely dashed lines). Note that the responses to sinusoidal perturbations are smaller than the responses to pulses and have been plotted on a different amplitude scale. Amplitudes for the two kinds of perturbations have been scaled so that they appear at a similar position on the *y*-axes for low stimulus amplitudes, to emphasize the difference in the degree of saturation.

Figure 4*D* shows the same general results from experiments on *monkey Mo*. Responses to sine waves showed more saturation (only 38% of the linear expectation) than did responses to pulses (59% of the linear expectation). For this experiment, sine wave perturbations were only one cycle long. *Monkey Mo* was used for this experiment only; all subsequent experiments use *monkeys Na* and *Ka*. The parameters of the logarithmic fits are given in the figure legend and, as expected, show a greater saturation for the fits to sine wave perturbation responses than for the fits to pulse perturbation responses. Linear regressions to the responses to sine waves showed *y*-intercepts significantly greater than zero (*Mo*, $P < 0.05$; *Na*, $P < 0.05$ for response to 1st cycle, $P < 0.005$ for response to all cycles), indicating that the response saturated. To determine whether the degree of saturation was significantly greater for sine waves than for pulses, we divided the response to the latter by the response to the former. This ratio was significantly larger for larger amplitude stimuli (*Mo*, $P < 0.05$; *Na*, $P < 0.05$ for response to 1st cycle, $P < 0.005$ for response to all cycles). While one expects the biphasic sinusoidal perturbations to evoke lower amplitude responses overall, relative to the pulse perturbations, some nonlinearity must be proposed to explain why they also evoke more response saturation.

Interaction of sinusoidal and pulse perturbations of target velocity

Our interpretation of the data in Fig. 4 is that the responses to high-frequency sine wave perturbations are driven largely by a fast-saturating sensitivity to image acceleration. While other interpretations are possible, this interpretation guided the design of the following experiment, which seeks to analyze the nature of the proposed saturation further. We asked how the response to a sine wave perturbation depended on the baseline image velocity at the time of the perturbation. Our purpose was to determine whether the response to image acceleration saturates with increasing image acceleration, or with increasing image velocity. In other words, is the saturation best approximated as $S(\mathrm{d}v/\mathrm{d}t)$ or as $\mathrm{d}[S(v)]/\mathrm{d}t$, where v is image velocity and S is a saturating function? If the first possibility holds, then baseline image velocity should have no effect on the response to sinusoidal perturbations. If the second holds, then the response amplitude should decrease with increasing baseline image velocity.

Figure 5 illustrates that the response to sinusoidal perturbations depended strongly on the size of a concurrent pulse. Responses were evoked by perturbations that consisted of a single cycle of a 10-Hz sine wave superimposed on different amplitude 100-ms velocity pulses, all presented during maintained pursuit of target motion at 15°/s (methods shown in Fig. 3*D*). To isolate the response to the sine wave and exclude the response to the pulse itself, we computed the difference between the response to the sine wave with pulse (stimulus

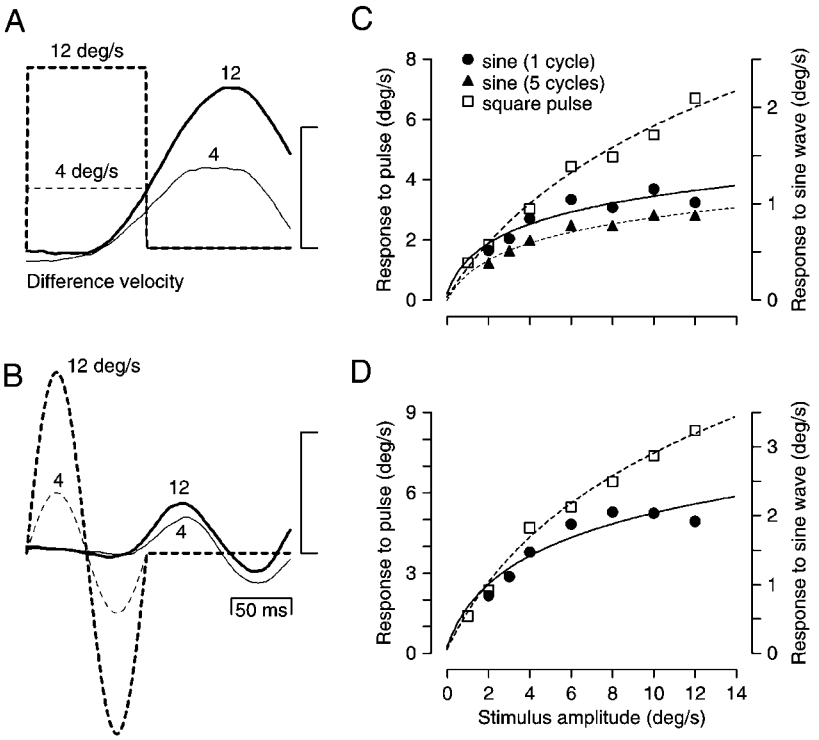

FIG. 4. Time courses and amplitudes of isolated responses to perturbations of target velocity imposed during pursuit of a 15°/s target. *A*: average difference eye velocity of *monkey Na* (solid lines) is plotted as a function of time, showing responses to 100-ms target velocity pulses (dashed lines) of 4°/s (fine lines) and 12°/s (bold lines). The scale bar is 4°/s for eye velocity and 8°/s for target velocity. *B*: same as in *A*, but responses are to the 1st 100 ms of sine wave perturbations with amplitudes of 4 and 12°/s. *C*: amplitudes of the responses of *monkey Na* are plotted vs. perturbation amplitude. □, amplitude of the responses to velocity pulses, plotted relative to the left-hand axis; ● and ▲, amplitude of the responses to sine waves, plotted relative to the right-hand axis; ●, amplitude of the response to the 1st 100-ms cycle. ▲, amplitude of the response for all 5 cycles. *D*: similar plot for *monkey Mo*. For *Mo*, sine wave perturbations were always only 1 (100 ms) cycle long, so only the responses to the 1st cycle are shown. Fits in *C* and *D* were made using the function $g * \ln(kx + 1)$, where x is the input. For the fits to the circles, triangles, and squares in *C*, the values of g were 0.34, 0.33, and 4.8, and the values of k were 0.22, 0.12, and 0.023. For the fits to the circles and squares in *D*, the values of g were 0.77 and 5.3, and the values of k were 0.13 and 0.031.

shown in Fig. 3*D*, *3rd trace*) and the response to the pulse alone (Fig. 3*D*, *2nd trace*). The resulting difference traces in Fig. 5*A* show that the sinusoidal perturbation of target velocity caused very little modulation of eye velocity when the pulse of image velocity was either 4°/s in the direction of ramp target motion (trace labeled "4 deg/s") or 6°/s in the direction opposite target motion (trace labeled "−6 deg/s"). The amplitude of the response grew as the pulse size was reduced and was largest when the pulse was 2°/s in the direction opposite target motion (trace labeled "−2 deg/s"). Average eye velocity at the

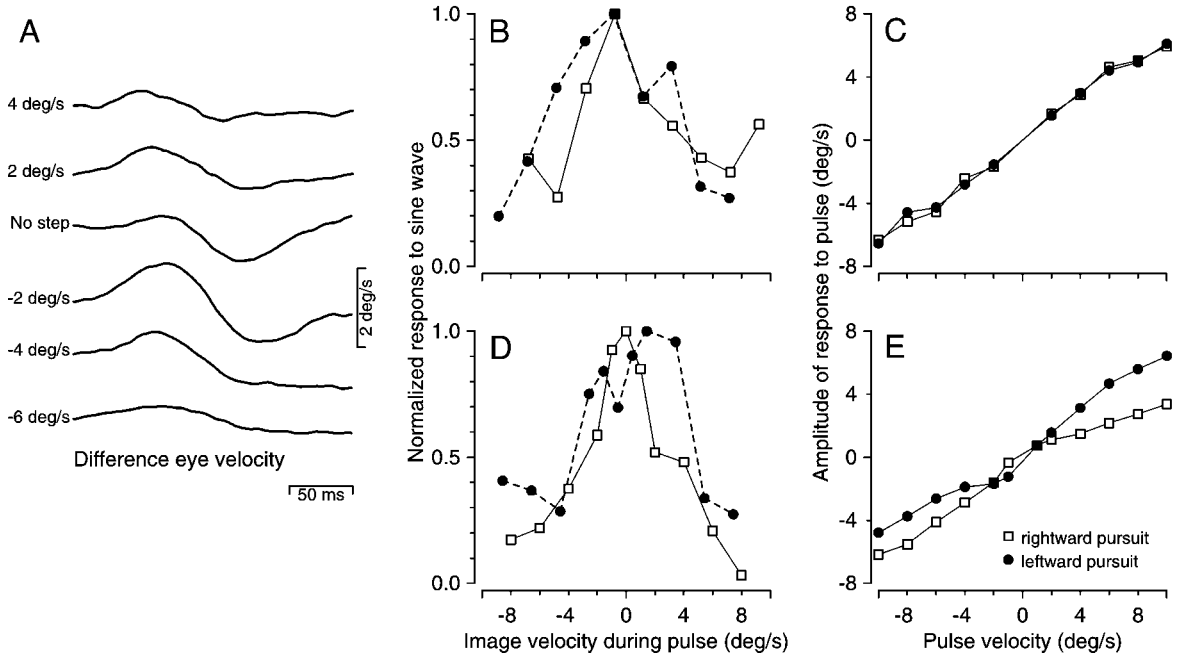

FIG. 5. Effects of different baseline image velocities on the response to sine wave perturbations of target motion. *A*: average difference eye velocity traces showing responses of *monkey Na* to a 10-Hz, ±2°/s sinusoidal perturbation. Numbers to the left of the traces indicate the amplitude of the pulse of target velocity on which sinusoidal perturbations were superimposed. Perturbations began 50 ms before the onset of the traces. *B* and *D*: amplitude of the response to the sinusoidal perturbation is plotted as a function of the baseline image velocity produced by the concurrent pulse for *monkeys Na* and *Ka*. Positive and negative values of image velocity created by the pulses correspond to rightward and leftward image motion, respectively. □ and ●, responses to perturbations imposed on rightward and leftward target motion, respectively. *C* and *E*: amplitude of the response to pulses of target velocity, plotted as a function of pulse size, for *monkeys Na* and *Ka*.

time of the perturbation was 13.8°/s, which is 1.2°/s smaller than the original 15°/s target velocity. Thus the image velocity offset caused by the pulse was smallest during the −2°/s pulse, when the response to the sine wave was largest.

Figure 5, *B* and *D*, summarizes, for *monkeys Na* and *Ka*, the finding that the response amplitude depended strongly on the mean image velocity during the perturbation. Response amplitude is shown normalized by its maximum value. The amplitude was largest when the mean image velocity was near zero, and declined sharply with increasing image velocity in either the same or opposite direction from target motion. This decrease was significant for both monkeys (linear regression, $P < 0.001$ for both). These results support the hypothesis that high-frequency sine wave perturbations are driven in part by a sensitivity to image acceleration, and that this sensitivity saturates with increasing image velocity. That is, the saturation is best expressed as $d[S(v)]/dt$. However, the results of Fig. 5, *B* and *D*, could also have been obtained if sine wave perturbations are driven purely by a strongly saturating sensitivity to image velocity. To test this possibility, we assessed the linearity of the pursuit response to pulses of target velocity presented alone. Control trials presenting pure pulses were interleaved with experimental trials.

The responses to pulse perturbations are summarized in Fig. 5, *C* and *E*. As in Fig. 4, the response to pulses alone saturated only moderately with increasing stimulus amplitude. For *monkey Na* (*C*), the response to an 8°/s pulse was 76% of the linear expectation given the response to a 2°/s pulse. This mild saturation is unlikely to account for the results of *B*, where sine wave response amplitudes fell to less than one-half when image velocity was between 4 and 8°/s. *Monkey Ka* (*E*) showed an asymmetry: considerable response saturation was observed only when the pulse increased target velocity (*right-hand side* for the open squares plotting rightward pursuit, *left-hand side* for the filled circles plotting leftward pursuit). The response to an 8°/s decrease in target velocity was 88% of the linear expectation, while the response to an 8°/s increase was only 58% of the linear expectation. This asymmetric response saturation is almost certainly due to eye velocity saturation and cannot account for the responses of *monkey Ka* in *D*, where response amplitude decreased similarly regardless of whether the pulse increased or decreased eye velocity.

Given that the response to sinusoidal motion is reduced by the addition of image velocity, one would expect that the natural fluctuations in image velocity during pursuit maintenance might have a similar influence. Perturbations presented when eye velocity is near the baseline target velocity would evoke larger responses than perturbations presented when eye velocity is farther from the baseline target velocity. To test this hypothesis, we pooled data from a number of experiments using 10-Hz perturbations (those shown in Figs. 4, 5, and 8, along with others not shown in this paper). For each experiment, we calculated the average absolute image velocity, across all trials, during the time the perturbation was presented. Within each experiment, we then divided individual trial responses into two bins: one in which baseline image velocity at the time of the perturbation was higher than average, and one in which baseline image velocity was lower than average. The trials in each bin were then averaged, and the response to the perturbation was calculated as described above. It was necessary to bin and average because responses were obscured by noise in the majority of individual trials, and were clear only in the averages. For *monkey Na*, image velocity averaged 2.4°/s for the first bin and 0.9°/s for the second (averages over 16 experiments). The response to a 10-Hz sinusoidal perturbation was on average 34% smaller in the first bin (2-tailed *t*-test, $P < 0.0002$). For *monkey Ka*, image velocity averaged 1.7°/s for the first bin and 0.7°/s for the second (averages over 11 experiments). The response was on average 16% smaller in the first bin ($P < 0.05$). Thus even the small naturally occurring departures from zero image velocity that occur during pursuit maintenance can reduce the pursuit response to sinusoidal perturbations. For comparison, consider only those responses in Fig. 5, *B* and *D*, where image velocity during the pulse was <2°/s (mean = 1.1°/s) or >4°/s (mean = 6.4°/s). Across both directions and monkeys, the response in the latter condition was 59% smaller (standard error = 6%).

Closed loop responses to steps and sinusoidal perturbations of target velocity

To provide a data set for testing the models under closed-loop conditions, we conducted modified versions of experiments already in the literature. We recorded the responses of *monkeys Na* and *Ka* to 15°/s steps of target velocity, and to multi-cycle sine wave perturbations over a range of frequencies from 1 to 10 Hz. Sine wave perturbations were imposed during maintained pursuit of 15°/s steps. Perturbations were presented in the minority (25%) of trials; target velocity was usually a pure 15°/s step.

Figure 6 shows 12 responses of *monkey Na* to a 15°/s step of target velocity. For this monkey, spontaneous oscillations at approximately 5 Hz were a typical, if not universal (see *examples 11* and *12*) feature of maintained pursuit. However, comparison along the vertical dashed line reveals that the phase of these oscillations was not consistent between trials. As a result, the average eye velocity response, when aligned on the onset of target motion, showed no spontaneous oscillations (e.g., Fig. 3*B*). For comparison of different models, we did not wish to use average responses that were unrepresentative of the majority of individual responses. We wished particularly to preserve the spontaneous oscillations present in individual trials, since fitting the oscillation period has been an important challenge for models of pursuit (Goldreich et al. 1992; Ringach 1995; Robinson et al. 1986).

Our solution to this problem, shown in Fig. 7, was to make two averages: one with individual trials aligned on the initiation of pursuit, and a second average aligned on the first trough of the spontaneous oscillations. Most records exhibited at least one full oscillation cycle, making this strategy feasible. For the few trials that did not show any clear oscillations, we made an estimate based on the end of the initial eye acceleration and the typical period of the oscillations. After obtaining the two averages, we spliced them at the point were their accelerations and velocities were both equal, just before the end of the initial eye acceleration. The resulting "spliced average" (Fig. 7) was representative of both the initial eye acceleration and the typical amplitude and period of the spontaneous oscillations, and was used as the goal for the models' responses. The spliced average is related to the method used by Robinson et al. (1986) to solve the same problem. For these experiments, we had many more repetitions of the responses to steps of target

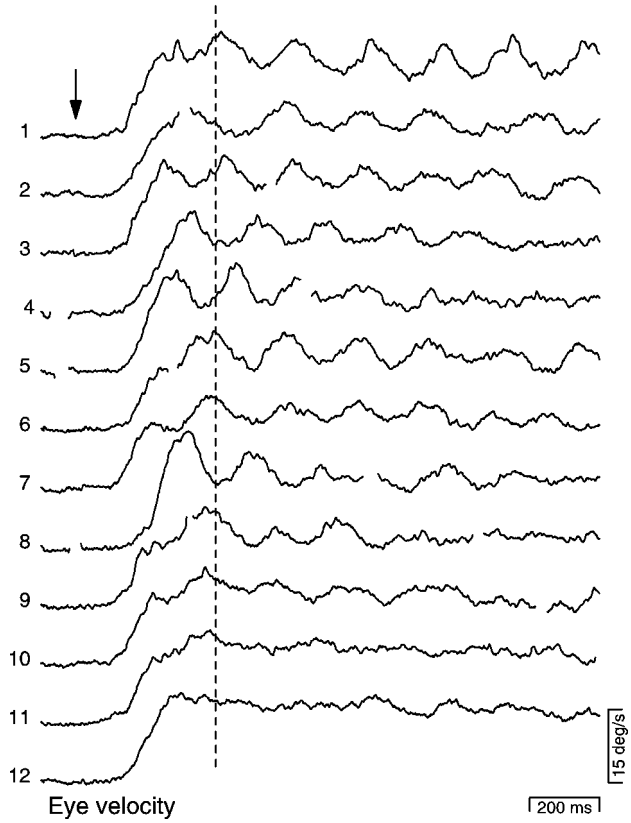

FIG. 6. Eye velocity traces of *monkey Na* illustrating the variation in the phase and amplitude of oscillations in individual responses. The stimulus was a step-ramp of target position that provided a step of rightward target velocity at 15°/s. The downward arrow indicates the onset of target motion, and the vertical dashed line is placed 400 ms later to aid comparison of the phase of oscillations. Saccadic deflections of eye velocity have been excised but not replaced.

velocity than we needed. Therefore we averaged only a randomly selected subset of 25–35 repetitions.

Figure 8*A* shows the spliced averages of eye velocity (—) for *monkey Na* to rightward and leftward 15°/s steps of target velocity (- - - - -). We estimated the feedback delay of this

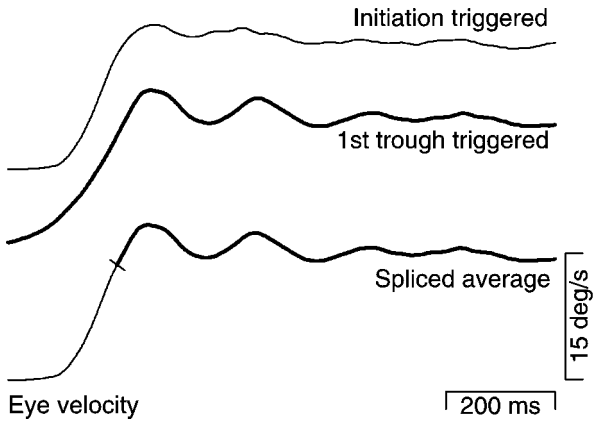

FIG. 7. Average eye velocity traces showing how we created a goal for the models that was representative of individual trial behavior. The *top trace* shows the average of eye velocity aligned at the onset of pursuit. The *middle trace* shows average eye velocity aligned on the 1st trough in the eye velocity oscillations. The *bottom trace* shows a spliced average, made by connecting the top 2 averages at the point where their velocity and acceleration were both equal. The tick mark orthogonal to the spliced eye velocity trace shows the time of the splice.

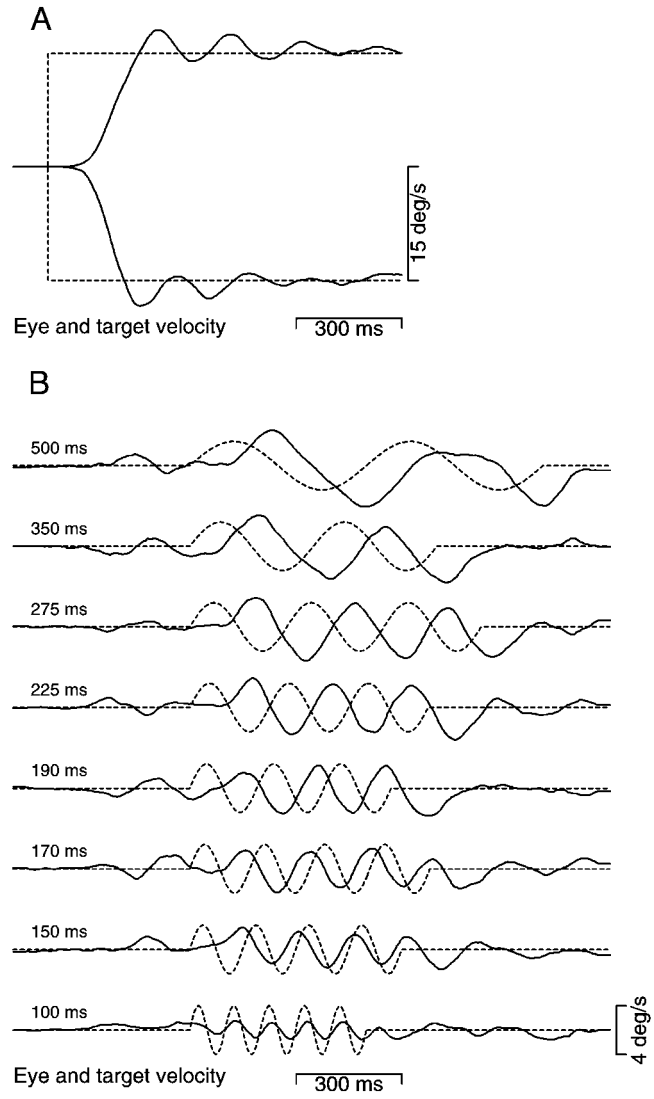

FIG. 8. Average responses of *monkey Na* to target motion at constant speed and to sine wave perturbations of target velocity. *A*: spliced averages (—) for rightward and leftward 15°/s steps of target velocity (- - - - -). *B*: difference eye velocity (—) and target velocity (- - - - -) showing the responses to ±2°/s sine wave perturbations of different periods. Numbers to the left of each trace indicate the period of the sine wave perturbation.

monkey's pursuit system to be about 80 ms, based on the latency to respond to perturbations of target velocity imposed during maintained tracking. The spontaneous oscillations were lightly damped and persisted for several cycles with a period of 207 ms, a little over twice the feedback delay. In contrast to *monkey Na*, *monkey Ka* exhibited spontaneous oscillations in only a small subset of his responses (individual responses not shown). Thus aligning his responses on the onset of target motion produced average responses that resembled individual responses. However, we found that by averaging his responses time locked to the peak of the usual small overshoot of target velocity, we better preserved this aspect of individual responses. Responses of *monkey Ka* are shown alongside those of the models in Fig. 13*A*. On rare occasions when spontaneous oscillations were present in the individual responses of *monkey Ka*, their period was around 150 ms, just over twice the estimated feedback delay of 65–70 ms.

Figure 8*B* shows the responses of *monkey Na* to sinusoidal

perturbations over a range of frequencies, collected during the same experiment as the step response in *A*, and isolated as described in METHODS. As expected, eye velocity (—) always lagged target velocity (- - - - -), even for 500-ms period perturbations (2 Hz). As the period of the sinusoidal perturbations decreased, the phase lag increased until it exceeded 360° for perturbations with a period of 100 ms. In agreement with previous data (Goldreich et al. 1992), the gain of the response was close to one for 500-ms period perturbations (2 Hz), and declined to somewhat less than 0.5 for 100-ms period perturbations (10 Hz). One feature of these responses is particularly notable, even though it can be predicted from the unexpected stability of pursuit in the face of artificially increased feedback gains (Robinson 1965). Given the lightly damped spontaneous oscillations in response to steps of target velocity, linear systems analysis predicts that the system should resonate strongly when stimulated at the oscillation frequency. The amplitude of the eye velocity response should increase with each cycle of the perturbation, and the final gain should be quite high. This did not occur. In Fig. 8*B*, the gain of the response to a perturbation of period 190 ms is less than one and is smaller than that to a perturbation of period 350 ms. However, the absence of the resonance predicted by linear control models is perhaps not surprising, as we observed above that the pursuit response to sinusoidal target motion is far from linear. In particular, fluctuations of eye velocity about target velocity (as in Fig. 6) increase baseline image velocity and are thus expected, given the data in Fig. 5, to reduce the response to sinusoidal perturbations.

The responses of *monkey Ka* to sinusoidal perturbations of target velocity were similar to those of *monkey Na* and are shown later (Fig. 13*C*). Again, there was no pronounced increase in the response gain when the perturbation frequency was near that of the (rarely observed) spontaneous oscillations.

Architecture of the models

Both the image motion model (Goldreich et al. 1992; Krauzlis and Lisberger 1989, 1994b) and the tachometer feedback model (Ringach 1995) attempt to explain why pursuit eye velocity follows trajectories like those in Fig. 2, *B* and *C*, rather than that of a simple velocity servo as in Fig. 2*D*. For the image motion model, the use of image acceleration (and deceleration) information limits the overshoot of target velocity and produces the correct oscillation frequency of approximately twice the visual feedback delay. Intuitively, performance of the simple velocity-servo model is poor because what is needed to ensure perfect performance is current image velocity, $\dot{I}(t)$, while what is available is a delayed image velocity signal, $\dot{I}(t - \Delta t)$. The image motion class of models essentially makes the first-order estimate: $\dot{I}(t) \approx \dot{I}(t - \Delta t) + g\ddot{I}(t - \Delta t)$. For the estimate to be optimal, g should be approximately Δt. If the image acceleration signal is too weak, large overshoots will result. If it is too strong, spontaneous oscillations are produced with a period of twice the visual delay. These spontaneous oscillations represent repeated over-corrections. The period is twice the delay because one delay interval expires between maximum image acceleration (maximum eye deceleration), and the maximum of the subsequent overcorrecting response: maximum eye acceleration. The response delay thus accounts for one-half cycle, from maximum eye deceleration to maximum eye acceleration. These explanations are complicated somewhat by the addition of filters and of nonlinear gain elements, but remain a fruitful way of understanding the behavior of the image motion model. A formal explanation of these effects can be found in the Appendix of Goldreich et al. (1992).

Figure 9*A* shows a block diagram of a revised image motion model. Target velocity ($\dot{T}$) and eye velocity ($\dot{E}$) are compared by the model at a summing junction that represents the retina, yielding image velocity ($\dot{I}$). Image velocity is then processed in three parallel pathways. The outputs from the three visual pathways are eye acceleration commands that are summed and mathematically integrated to create a command for eye velocity ($\dot{E}$). The eye velocity command is then passed through a low-pass filter (labeled "plant") to yield actual eye velocity ($\dot{E}$). The relatively simple dynamics of the plant are based on the widely accepted idea that neural circuits not included in our model compensate for the physical dynamics of the eye (Skavenski and Robinson 1973).

The top visual pathway in Fig. 9*A* takes image velocity as its input, delays it, processes it with a nonlinear gain element, and subjects it to low-pass filtering with a single time constant. The middle pathway has the same three elements (with different parameters), plus a switch that is on only for 30 ms following the onset of target motion, to produce a "Motion onset transient." This pathway was included to account for certain nonlinearities present during the initiation of pursuit, but is silent during maintained pursuit, and is thus of minor relevance to the majority of our analysis. The bottom pathway receives an image velocity input that is first delayed and passed through a saturating nonlinearity. The derivative is then taken, and the resulting image acceleration signal then passes through a second nonlinear gain element and filter. An additional low-pass filter is associated with the differentiation.

The model in Fig. 9*A* has three departures from the image motion model of Krauzlis and Lisberger (1994b). First, it adds a nonlinearity to the acceleration pathway, situated before the derivative of image velocity is taken. This nonlinearity was crucial in fitting much of the data presented in this paper and was motivated by the data in Figs. 4 and 5. When set to saturate, the nonlinearity reduces the sensitivity to image acceleration when image velocity is high; an acceleration from 0 to 5°/s produces a larger output than does the same magnitude acceleration from 30 to 35°/s. Second, each of the parallel pathways now has an independent time delay. These delays were allowed to vary slightly from one another (see Table A1) to achieve the best fit to the data. Third, the current model does not use temporal filters with inherent resonance. Given that relatively little is known about the filtering properties of the pursuit system, we made the simplest possible assumption and used low-pass filters described by a single exponential time constant.

We converted the image motion model into an equivalent tachometer feedback model by replacing the image velocity input to the acceleration pathway with a negative eye velocity input. The tachometer feedback model, shown in Fig. 9*B*, shares the first two pathways with the image motion model. However, the bottommost pathway embodies a sensitivity to eye acceleration, rather than a sensitivity to image acceleration. This version of the tachometer model uses potentially nonlinear gain elements and is capable of showing all the features of

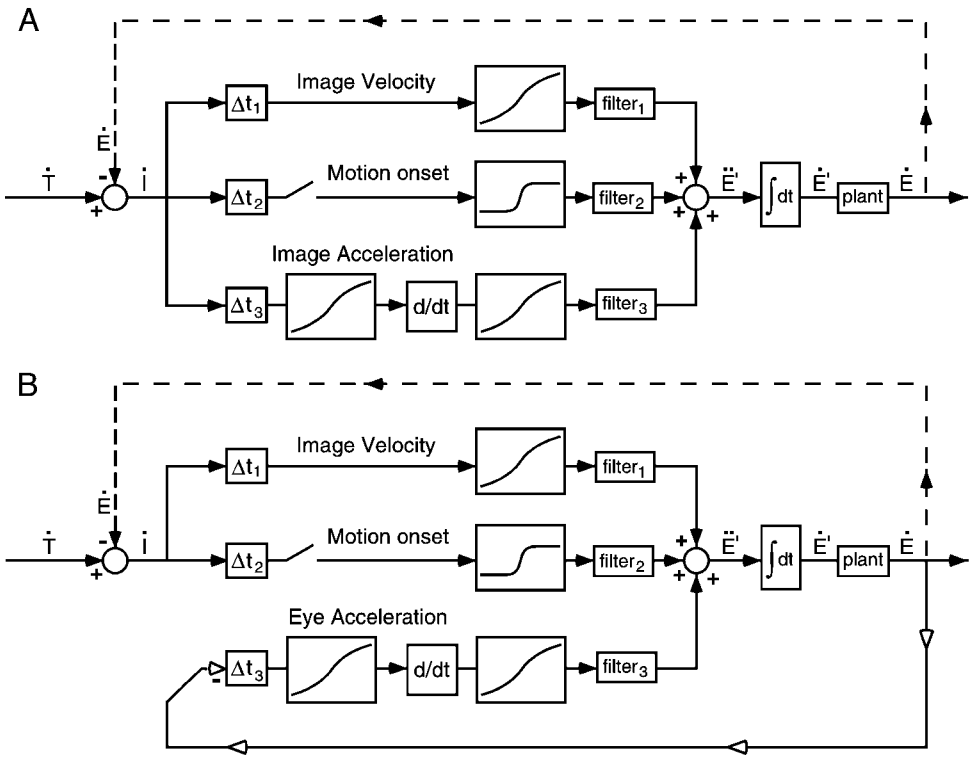

FIG. 9. Architecture of the image motion model (*A*) and the tachometer feedback model (*B*). Inputs arise on the *left* and outputs are shown on the *right*. Solid lines show the flow of signals within the pursuit system. The dashed line reflects negative feedback that results because the retina is attached to the moving eye. Circular nodes operate as summing junctions. The input to both models is retinal image velocity İ, obtained by taking the difference between target velocity, Ṫ, and eye velocity, Ė. Each model contains 3 pathways whose outputs are summed to generate an eye acceleration command. The top 2 pathways are the same for the 2 models and receive an image velocity input. For the image motion model, the bottom pathway also receives an image velocity input. For the tachometer feedback model, the bottom pathway receives an eye velocity input. Each pathway contains a delay, labeled as Δt, a filter, and one or more nonlinear gain elements. The middle pathway also contains a switch so that it is active only for the 1st 30 ms after the target begins to move. The bottom-most pathway adds a 2nd nonlinear gain, situated prior to differentiation of the input signal. The outputs of the 3 pathways are summed to create the net eye acceleration command, Ë, which is integrated to produce an eye velocity command, Ė. This command then passes through a final filter, labeled "plant," to yield actual eye velocity, Ė.

the original linear tachometer model and more. The inclusion of the motion onset pathway does confer a limited type of image acceleration sensitivity (at the onset of target motion) to the tachometer feedback model. However, we felt this pathway should be included given the ample evidence for a motion onset transient that drives eye acceleration at the initiation of pursuit (Krauzlis and Lisberger 1994a; Lisberger and Westbrook 1985). To further facilitate comparison of the two models, we designed the differentiator in the acceleration pathway of the image motion model to ignore the brief pulse of image acceleration present when the target first began to move. Any response to motion onset could still be modeled by the motion onset pathway.

The two models are functionally nearly identical for target motion at a constant velocity. Eye deceleration is identical to image acceleration when target acceleration is zero, and the eye acceleration pathway of the tachometer feedback model thus has a similar effect on model performance as does the image acceleration pathway of the image motion model. The only differences arise due to the potentially nonlinear gain that precedes differentiation within the acceleration pathway. The nonlinearity acts on image velocity for the image motion model, and on eye velocity for the tachometer feedback model, and image velocity is typically not equal to eye velocity. In general, optimized versions of the tachometer feedback model tended to use a nearly linear transfer function in this position, while the image motion model used a saturating nonlinearity. Still, the performance of the two models was nearly identical for steps of target velocity. The two models produced dramatically different responses *1*) when the target accelerated continuously and *2*) when visual feedback was artificially delayed. The latter condition creates different predictions for the two models because it delays both types of feedback (image velocity and image acceleration) for the image motion model, but only the image velocity feedback for the tachometer feedback model.

We have diagrammed the architecture of the models to highlight their close formal relationship. In doing so, we have lumped into the total delay of each pathway a motor delay that in Ringach's original formulation affected the final common pathway. This formulation of the delays is formally identical to the original. As described, the models employed many free parameters, eight describing the delay and filtering properties of pursuit, with multiple additional parameters describing the four nonlinearities. The number of free parameters may seem excessive, and indeed it was designed to be. We wished to ensure that any failings of the models were due to limitations imposed by their architecture, and not to a lack of free parameters.

Simulation of open-loop responses

The simulations shown in Fig. 10*A* verify our earlier conclusion that a saturating response to image acceleration is sufficient to account for the discrepancy in response saturation between pulses and sine waves. There is excellent quantitative agreement between the output from the image motion model (Fig. 10*A*, —, - - - - -, and – – –) and the responses of *monkey Na* to pulse and sine wave perturbations of target velocity (symbols, replotted from Fig. 4). For both the model and the monkey, the response to pulses of target velocity (—, □) showed less saturation than did responses either to the first cycle of a 10-Hz sine wave (- - - - -, ●) or to all five cycles (– – –, ▲). The model and the monkey both showed slightly smaller response amplitudes when measured over five cycles instead of one. Model responses were obtained using target

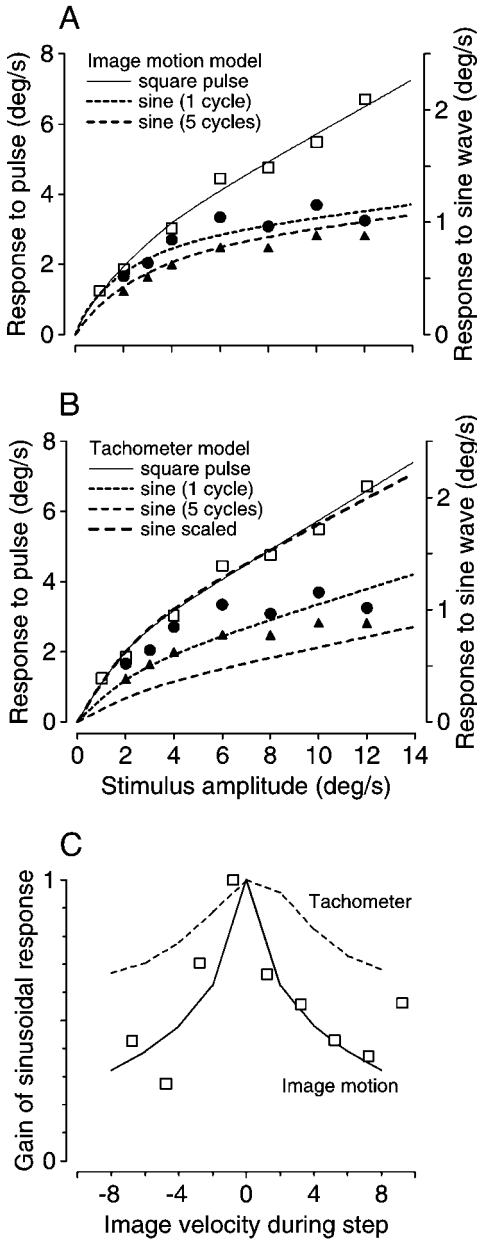

FIG. 10. Comparison of model and monkey responses to target velocity perturbations. *A* and *B*: the graphs plot response amplitude as a function of stimulus amplitude. Symbols show data for *monkey Na*, replotted from Fig. 4*A* for 100-ms pulses (□), 1 cycle of a 100-ms period sine wave (●), and 5 cycles of the same sine wave (▲). Curves of different weights show attempts to fit the same data with the image motion model (*A*) and the tachometer model (*B*). In *B*, the top, longest-dashed curve is a replica of the tachometer model's performance for single cycles of a sine wave, scaled to emphasize that the saturation exhibited by the model was similar for pulses and sine waves. *C*: the gain of the response to a sine wave perturbation is plotted as a function of baseline image velocity created by a concurrent pulse. Open squares replot the data shown by the open squares in Fig. 5*B*. Curves show the best fits for the image motion model (solid lines) and the tachometer feedback model (dashed lines). The data in Fig. 10*C* were collected on a different day than those in Fig. 10*A*, and slightly different parameters were used to provide fits. These parameters are not shown in Fig. A1 or Table A1 but were similar to those used for the simulations in Fig. 10*A*.

velocity inputs equal to the sine wave or pulse perturbation of interest. Response gains were then calculated just as they had been for the monkey. To fit these data, the image motion model relied on the combination of a nearly linear response to image velocity, and a response to image acceleration that saturated with increasing image velocity. The parameters used to achieve these fits are reported in Fig. A1 and Table A1.

The tachometer feedback model was less successful in reproducing the responses to pulse and sine wave perturbations of target velocity. When the parameters were set so that the responses to pulses were fit well (Fig. 10*B*, —), the gain of the response to sine waves was too low for all but the highest stimulus amplitudes (bottom 2 dashed lines). This was especially true when all five cycles of the response were considered (bottom dashed line). In addition, the response of the model did not saturate quickly enough with increasing sine wave perturbation amplitude. Scaling the responses of the model so that the pulse and sine wave response gains overlap for low amplitude stimuli (top dashed line) reveals that the response to sine waves saturated to the same degree as the response to pulses. It was possible to configure the tachometer feedback model to produce responses to sinusoidal perturbations with the appropriate gain and saturation. However, the model's responses to velocity steps were then too large and exhibited far too much saturation (simulation data not shown). As discussed later, these shortcomings are due not to the use of motor feedback, but to the tachometer model's lack of sensitivity to image acceleration.

We also fit both models to the responses of *monkey Na* to sine waves imposed on velocity pulses, and to his responses to the pulses alone, originally shown in Fig. 5. As in Fig. 10, *A* and *B*, both models were able to reproduce accurately the responses to different amplitude pulses (simulation data not shown, but fits were as good as in Fig. 10, *A* and *B*). However, only the image motion model was also able to reproduce the responses to sine waves presented on top of pulses. Figure 10*C* shows, for the two models (curves) and for the monkey (symbols), the response gain for sine waves as a function of the mean image velocity created by a concurrent pulse. The responses of the models were isolated using the same method employed for the behavioral data: the response to the pulse alone was subtracted from the response to the pulse/sine wave combination. The image motion model (—) captures the steep decline in response gain with increasing image velocity (□). The behavior of the image motion model is due to the initial nonlinearity in the image acceleration pathway (bottom pathway of Fig. 9*A*). When baseline image velocity is zero, the input to the pathway engages the steep part of the nonlinearity, and the signal to be differentiated has a relatively high gain. When baseline image velocity is either above or below zero, the input to this pathway engages the shallower part of the nonlinearity, and the signal to be differentiated has a relatively low gain. In effect, the gain of the image acceleration pathway varies as a function of baseline image velocity.

The tachometer feedback model (- - - - -) showed only a modest decline in response gain with increasing baseline image velocity. The decline was due to the saturation of the response to image velocity. The tachometer model was able to produce a steeper decline, but only if its responses to pulses saturated much more than did the monkeys' (simulation data not shown). Because the data are expressed in normalized form, Fig. 10*C* obscures an additional failure of the tachometer feedback model; when image velocity was zero, the responses of the tachometer feedback model to sinusoidal perturbations of tar-

get velocity were only 50% as large as those of the monkey. The data from *monkeys Mo* and *Ka* were sufficiently similar to those of *monkey Na* that we did not repeat the simulations using their data as a goal.

Simulation of closed-loop responses under conditions of delayed visual feedback

We next ask whether the nonlinear visual properties of our elaborated image motion model are sufficient to explain pursuit under closed-loop conditions, or if sources of motor feedback must also be assumed. Ringach has argued that the image motion model is unable to account for some aspects of pursuit under conditions of delayed visual feedback, and indeed this is true for a linear model. We now compare the behavior of the *nonlinear* versions of both models with the pursuit behavior that led Ringach to reject the *linear* image motion model. The solid lines in Fig. 11 reproduce data from Goldreich et al. (1992) and show responses of a monkey to a 15°/s step of target velocity, with artificially imposed feedback delays indicated by the numbers to the left of each trace. As reported in detail before, and as expected from an image motion model, the period of the spontaneous oscillations increased with feedback delay. The increase is not linear, however. At short artificial delays the oscillation period is approximately twice the total feedback delay, while at long artificial delays the period is closer to four times the total feedback delay. There is also an increase in the damping of the oscillations at intermediate delays. These more subtle aspects of the data could not be reproduced by a linear image motion model (Ringach 1995), although it has previously been shown that a nonlinear image motion model can produce a nonlinear increase in oscillation period with increasing feedback delay (Krauzlis and Lisberger 1994b).

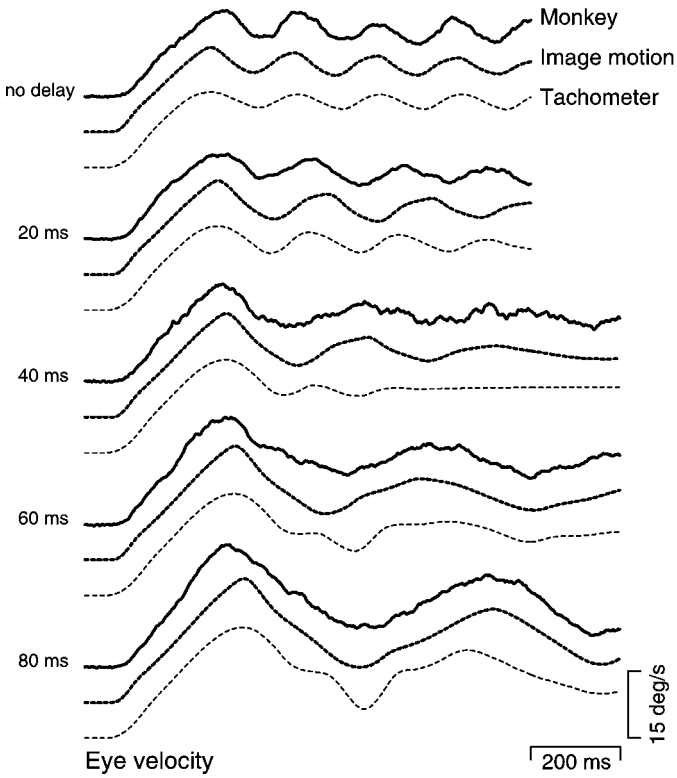

FIG. 11. Comparison of eye velocity responses of *monkey Jo* (solid lines) under conditions of artificially delayed visual feedback with the output of the image motion model (thick dashed traces) and the tachometer feedback model (thin dashed traces). Target motion was a 15°/s step of target velocity. Numbers to the left of each trio of traces indicate the amount of added feedback delay. Experimental data are reproduced from Fig. 3 of Goldreich et al. 1992.

The dashed traces in Fig. 11 show that the nonlinear versions of both models provide good fits to the data of Goldreich et al. (1992). Both models show realistic effects of increases in feedback delay with respect to the oscillation period and the damping. Thus the primary criticism leveled by Ringach (1995) against the linear image motion model is obviated by the nonlinear version of the model. The nonlinear image motion model succeeds where the linear version failed primarily because of the addition of image velocity saturation prior to the extraction of image acceleration (1st nonlinearity in bottom pathway, Fig. 9*A*). The image acceleration pathway dominates the model's dynamics when the visual delay is short and the oscillations (and resulting image velocities) are small. Dominance of the image acceleration pathway produces an oscillation period roughly twice the feedback delay, as discussed above. When the visual delay is long and the oscillations (and resulting image velocities) become large, saturation weakens the image acceleration pathway, and the image velocity pathway dominates the dynamics, creating an oscillation period of roughly four times the feedback delay. Between these extremes is a period where the two pathways are more balanced, and damping is increased. The parameters that produced these fits are shown in Table A1, and the nonlinearities appear in Fig. A1.

The principle frequency of the spontaneous oscillations exhibited by the tachometer feedback model increases appropriately with increasing feedback delay, as described by Ringach (1995). However, for moderate to long delays, higher frequency oscillations produced by the eye acceleration feedback pathway, whose delay is unaltered, are superimposed on the lower frequency oscillations produced by the image velocity pathway. The model oscillates at two distinct frequencies. In contrast, the average responses of the monkey did not show two frequencies of oscillation. Although it is possible that high-frequency oscillations were present in individual trials and were lost due to averaging, this seems unlikely because for this monkey similar high-frequency oscillations were visible in the average responses when the visual feedback was not delayed. Unfortunately, the raw data from Goldreich et al. (1992) are no longer available to investigate directly the presence or absence of simultaneous oscillations at both high and low frequencies. For the responses of the image motion model, there are also some small departures from smoothness that appear as if they might represent a small higher frequency component. In fact, these result from a small discontinuity at zero in the derivative of the first nonlinearity in the image acceleration pathway (curve labeled "Image velocity #2" in the *2nd row* of Fig. A1). These small bumps would have been eliminated if we had parameterized the curve to allow asymmetry without a discontinuity in the first derivative.

Simulation of closed-loop responses to steps and sinusoidal modulations of target velocity

The image motion model was able to replicate the very different responses of *monkeys Na* and *Ka* to 15°/s steps of

target velocity (Figs. 12*A* and 13*A*). Different parameters were used in fitting the responses of the two monkeys (see Table A1 and Fig. A1), a necessity given their very different profiles of pursuit. The tachometer feedback model was equally successful in fitting the responses to steps of target velocity (Figs. 12*B* and 13*B*). These results were expected: the two models are formally very similar under these conditions, and both had previously been shown to successfully emulate pursuit of target velocity steps.

We next ask how well the models reproduce the responses to sinusoidal perturbations. For each monkey, responses to sine wave perturbations were collected during the same experimental session as the responses to steps. We simulated responses by simply providing the target velocity perturbations themselves as the input to the models. This method ignores the fact that, for actual pursuit image, velocity was rarely zero at the time the perturbations were imposed, due to imperfections in pursuit maintenance and the presence of spontaneous oscillations. The method essentially assumes that pursuit maintenance was perfect at the time of the perturbation. This choice of method avoided the myriad complications of attempting to incorporate noise sources into the models, but it posed a different problem. For a *linear* model, the average perturbation response would not depend on the presence of random-phase fluctuations in baseline image velocity. The versions of the two models we employ are not linear, but considering the small (1–2°/s) size of fluctuations in baseline image velocity during pursuit, the departures from linearity are expected to be of little consequence, with one key exception. For the image motion model, even small fluctuations in baseline image velocity will reduce the effective gain of the image acceleration pathway. One would therefore predict that the image motion model, configured to reproduce the response to steps of target velocity, would successfully reproduce the responses to sinusoidal perturbations if and only if the gain of the image acceleration pathway is reduced. This is precisely what we found.

The responses of the image motion model to sinusoidal perturbations are shown in Figs. 12*C* and 13*C*. The simulated responses successfully capture both the amplitude and the phase of the monkeys' responses. To achieve these fits, the gain of the image acceleration pathway was reduced, respectively, by 34 and 38%, relative to the gain that reproduced the step responses shown in Figs. 12*A* and 13*A*. Fluctuations in baseline image velocity are expected to have little or no effect on the duration of the visual delay, or on the effective gain of the image velocity pathway (which is nearly linear in the relevant range). All other parameters were therefore restricted to be the same when simulating responses to target velocity steps and perturbations. The reductions in gain were achieved by simply reducing the output of the image acceleration pathway by the indicated percentage. This is equivalent to linearly scaling the second nonlinear gain function of that pathway (see Fig. A1).

The reduction in the gain of the image acceleration pathway (34 and 38% for *monkeys Na* and *Ka*) was chosen to produce optimal fits. An independent estimate can be made of the decrease in responsiveness expected given the fluctuations of image velocity. For the data in Figs. 12 and 13, we measured image velocity during the time the sine wave perturbations were presented, but for individual trials *without* perturbations (i.e., pure 15°/s steps of target velocity). Image velocity during this interval fluctuated about target velocity as in Fig. 6, and its absolute value averaged 1.4°/s for *monkey Na* and 1.0°/s for *monkey Ka*. For *monkey Na*, we reported above that increases in baseline image velocity of 1.22°/s, −1.16°/s (both artificially produced), and 1.5°/s (naturally occurring) reduced the response to sine waves by 34, 33, and 34%, respectively. These values are very similar to the value of 34% used by the model

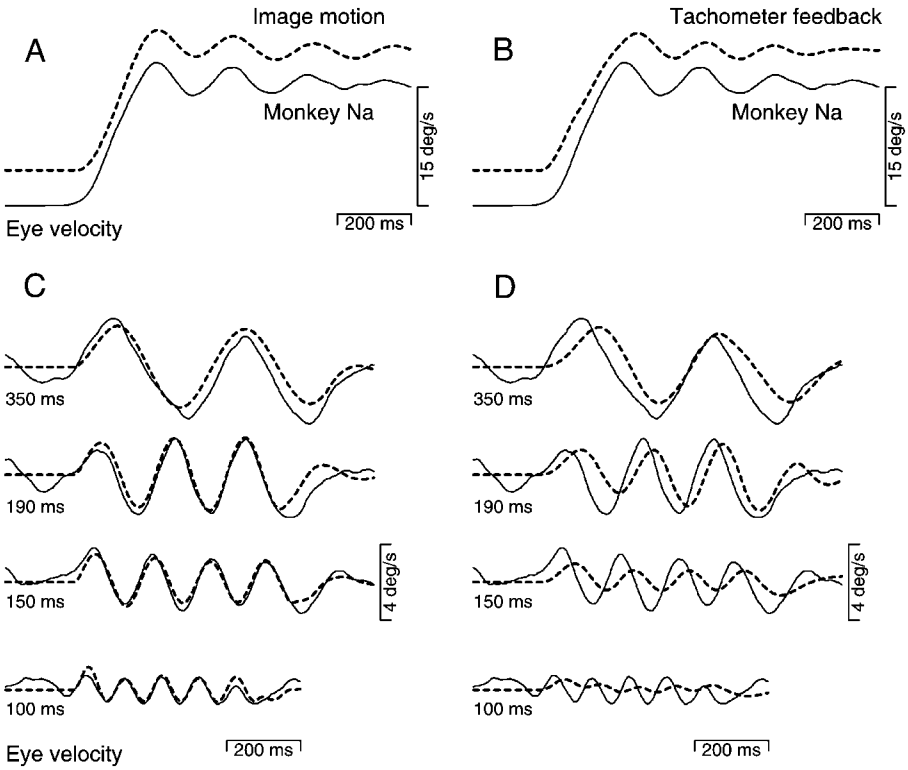

FIG. 12. Comparison of performance of *monkey Na* with the outputs of the image motion and tachometer feedback models. Dashed and solid traces show responses of model and monkey, respectively. Data are from *monkey Na* and are replotted from Fig. 8. *A* and *C*: image motion model. *B* and *D*: tachometer feedback model. In *A* and *B*, the stimulus was a step-ramp of target position that provided a step of constant target velocity at 15°/s. In *C* and *D*, the stimuli were sine wave perturbations of amplitude ±2°/s and of the period given by the numbers at the left of each trace. Model parameters are the same in *A* and *C*, except that the overall gain of the image acceleration pathway was reduced by 34% in *C*. Model parameters are the same in *B* and *D*, except that the overall gain of the eye acceleration pathway was reduced by 34% in *D*.

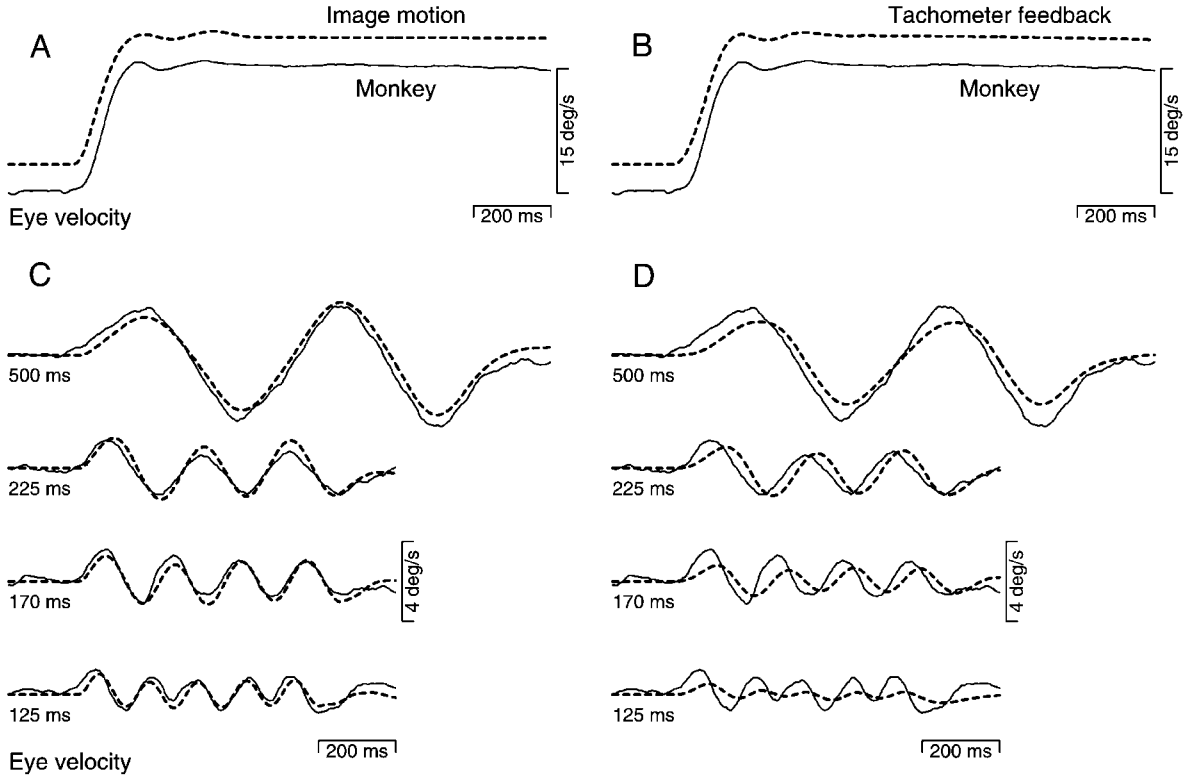

FIG. 13. Comparison of performance of *monkey Ka* with the output of the image motion and tachometer feedback models. *A* and *C*: image motion model. *B* and *D*: tachometer feedback model. Dashed and solid traces show responses of model and monkey, respectively. In *A* and *B*, the stimulus was a step-ramp of target position that provided a step of constant target velocity at 15°/s. In *C* and *D*, the stimuli were sine wave perturbations of amplitude ±2°/s and of the period given by the numbers at the left of each trace. Model parameters are the same in *A* and *C*, except that the overall gain of the image acceleration pathway was reduced by 38% in *C*. Model parameters are the same in *B* and *D*.

to fit the data of *monkey Na*. For *monkey Ka*, increases in image velocity of 1.0°/s, −1.0°/s (artificially produced), and 1.0°/s (naturally occurring) reduced the response by 15, 7, and 16%. These values are smaller than that used by the model (38%). In summary, although the decreases in responsiveness expected given the data are similar to the decreases in responsiveness necessary to allow the image motion model to achieve good fits, the two values do not agree exactly in both monkeys.

The responses of the tachometer feedback model were, like those of the image motion model, computed without regard to the fluctuations of image velocity during pursuit maintenance. The input to the model was simply the target velocity of the perturbation, as if maintenance were perfect. Unlike the image motion model, the presence of small fluctuations in image velocity do little to alter the behavior of the tachometer feedback model. Still, if we did not alter any parameters from the values that produced good fits to the responses to 15°/s steps, then the tachometer feedback model showed excessive resonance in its response to perturbations (these simulations are *not* those seen in Figs. 12*D* and 13*D*). We therefore allowed the optimization algorithm to use a lower gain for the eye acceleration pathway when fitting the tachometer feedback model to the perturbation responses to observe whether the tachometer feedback model exhibited any further failings, and to allow fair comparison with our simulations of the image motion model. In fitting the data of *monkey Na*, a 34% reduction in gain was used by the optimization algorithm. In fitting the data of *monkey Ka*, no change in gain was used. All other parameters were constrained to be the same for steps of target velocity and sinusoidal perturbations.

The responses of the tachometer feedback model to sinusoidal perturbations (Figs. 12*D* and 13*D*) differ from those of the monkeys in two ways. First, for all but the lowest frequencies, the response to sine wave perturbations showed excessive phase lag. Second, although the gain of the response was roughly appropriate for low frequencies, at high frequencies the responses were too small. Both of these failings can be traced to the tachometer feedback model's lack of image acceleration sensitivity, rather than to the presence of eye acceleration feedback. A hybrid model using both image acceleration and eye acceleration signals provided good fits (simulation data not shown), although not appreciably better than those provided by the pure image motion model.

Changes in the gain of the image velocity pathway also did little to improve the performance of the tachometer feedback model. If the response to high-frequency perturbations was made larger, then the response to low-frequency perturbations was overly large. The tachometer feedback model *could* reproduce the responses to sine waves for all frequencies, but only if the majority of the parameters were altered from the values that produced reasonable step responses. Excellent fits to sine waves were obtained by reducing the delay and filter time constant of the image velocity pathway, and by drastically reducing the delay of eye acceleration feedback, from 60–70 ms to 10–40 ms. However, such parameter changes made it impossible for the model to respond to 15°/s steps of target

velocity with the appropriate dynamics, or to produce spontaneous oscillations of the appropriate period. For the tachometer feedback model, the oscillation period is governed almost entirely by the delay of the eye acceleration pathway, and is approximately twice that delay. Repeated optimization attempts failed to fit the tachometer feedback model simultaneously to the responses to 15°/s steps and to sinusoidal perturbations, even when the eye acceleration pathway was allowed to have widely different gains for the two conditions. The simulations shown in Figs. 12 and 13 represent the best fits we were able to obtain.

Figure 14 summarizes the data in Figs. 12 and 13 and plots response gain and phase as a function of frequency for each monkey (□) and each configuration of the models. The best simulation of the data was provided by the image motion model, using the reduced image acceleration gain (▲). If we did not reduce the gain of the image acceleration pathway, the image motion model (△ for *monkey Na*) showed excessive resonance near the frequency of the spontaneous perturbations (vertical dashed line). For the tachometer feedback model (○) response gain was too low and phase lag too large for all but the lowest frequencies. The simulation responses analyzed in Fig. 14 were produced using the same parameters as in Figs. 12 and 13. Gain and phase were computed using the amplitude and phase of the relevant Fourier component, just as was done for the responses of the monkeys.

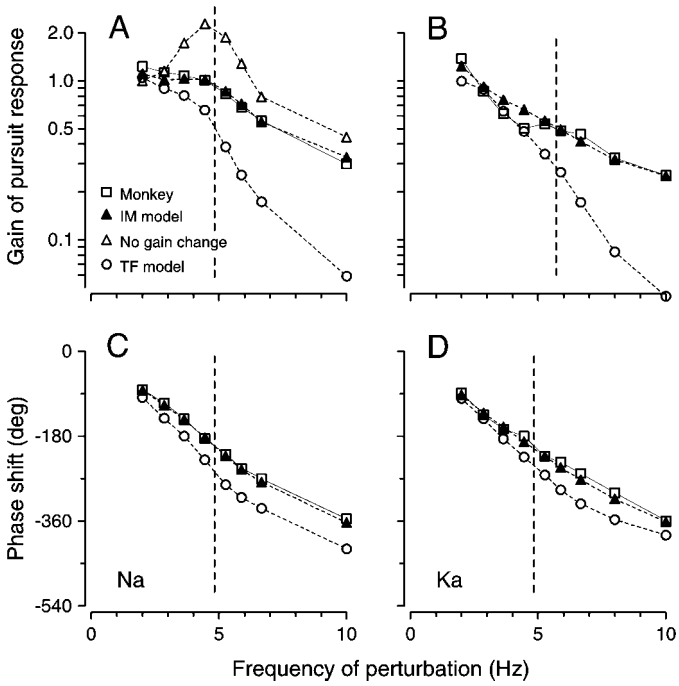

FIG. 14. Quantitative comparison of the responses of the monkeys and the 2 models to sine wave perturbations of target velocity. *A* and *B*: response gain is plotted as a function of stimulus frequency. *C* and *D*: phase shift between target and eye velocity is plotted as a function of stimulus frequency. *Left column*: *monkey Na*. *Right column*: *monkey Ka*. □, data from the monkey; ▲, data from the optimized image motion model; △, for *monkey Na* only, the data from the image motion model when the acceleration gain was held at the value that produced ideal fits for 15°/s velocity steps; ○, the responses of the tachometer feedback model. Vertical dashed lines indicate the frequency of the spontaneous oscillations during pursuit of target motion at constant velocity.

Model parameters

Because we desired accurate quantitative fits to large data sets, both models were simulated using a large number of free parameters and were allowed to use multiple nonlinear gain elements. The APPENDIX describes the parameters and nonlinearities that allowed the image motion model to reproduce the data in Figs. 10*A*, 11, 12, and 13. The use of multiple parameters and nonlinearities was important in providing precise quantitative fits. This is not surprising. The pursuit system itself exhibits a number of mild to profound nonlinearities. However, the exact shape of each nonlinearity should not be expected to capture exactly the corresponding nonlinear response property of pursuit. Not only are the nonlinearities somewhat under-constrained by our data, but changes in one can often partially compensate for changes in another. Nonetheless, for the one nonlinearity that can be measured in a model-independent fashion, the sensitivity to image velocity, the nonlinearities we used are very close to the measured functions (Krauzlis and Lisberger 1994a; Lisberger and Westbrook 1985; Morris and Lisberger 1987; Robinson et al. 1986).

Note also that the models are being asked to fit a number of responses, each of which is hundreds of milliseconds long. Past the open-loop interval, the response of the model depends on its previous behavior. Even very small failings will therefore tend to accumulate toward the end of the simulation. Multiple parameters and nonlinearities were necessary to achieve good quantitative fits. However, for the image motion model *qualitatively* appropriate behavior depended only on the saturation of image velocity prior to the extraction of image acceleration, and on reasonable choices for the visual delay. The version of the image motion model available on our website (http://keck.ucsf.edu/~sgl/top_pursuitmodel.htm) uses only a handful of free parameters and a single nonlinearity and can qualitatively reproduce pursuit behavior for all stimulus conditions described in this paper.

DISCUSSION

Nonlinearities of visual inputs and stability of pursuit

Pursuit relies on negative feedback, yet is remarkably stable given the long feedback delay. Pursuit does not break into uncontrolled resonance when driven at its natural frequency. Nor does it do so when the feedback delay is artificially increased. This stability is particularly surprising given that pursuit often appears to be on the verge of instability under more benign circumstances. Fuchs (1967) first noted that pursuit often breaks into spontaneous oscillations during tracking of a constant velocity target. In the current paper, such spontaneous oscillations were frequently present in the pursuit of *monkey Na*, and occasionally present in the pursuit of *Ka*. The responses of *monkey Jo*, reprinted from Goldreich et al. (1992) exhibit nearly undamped oscillations. It now seems fair to conclude that these oscillations are driven primarily by a sensitivity to image acceleration. The oscillation period (approximately twice the feedback delay) is consistent with this explanation, and nearly identical spontaneous oscillations are produced by the image motion model, due to its sensitivity to image acceleration.

As we have noted, the presence of spontaneous oscillations

gives way to an unfulfilled expectation of resonance for stimulus frequencies near that of the oscillations. The nonlinear response to image acceleration we document provides a potential explanation for the surprising stability of pursuit: the decline of image acceleration sensitivity with increasing image velocity acts to limit resonance. If oscillations, either spontaneous or driven, become too large, then the resulting image velocities reduce the tendency toward resonance. Even the initial response to perturbations is expected to be reduced by the presence of fluctuations in image velocity. The existence of this nonlinearity also has practical implications from the point of view of experimental design and interpretation. Many pursuit experiments employ changes in target velocity that are intended to probe the responsiveness of pursuit (Das et al. 1998; Krauzlis and Lisberger 1994a; Schwartz and Lisberger 1994). Our data make it clear that such experiments are difficult to interpret if the image velocity offset varies between the conditions being compared. For example, in Schwartz and Lisberger (1994) the conclusion drawn from Fig. 10, that the on-line gain of pursuit builds over the course of pursuit, is probably incorrect.

If fluctuations in image velocity during steady-state tracking reduce the response to sinusoidal perturbations, then the converse should also hold: creating fluctuations in image velocity *prior to* imposing a step of constant target velocity should reduce the presence of spontaneous oscillations in response to the step. This experiment was performed, although with different motivations, by Goldreich et al. (1992). They created ongoing sinusoidal target motion of a random phase, and then imposed a step of target velocity. By averaging across phases, they isolated the response to the step. For a linear system, this response should have been identical to the response recorded to the step alone, in the absence of sinusoidal target motion. Instead, as we predict, the tendency toward spontaneous oscillation was greatly reduced.

Summary of the comparison between models

We have found that an improved version of the image motion model is able to account for open-loop pursuit responses to velocity pulses, sine wave perturbations, and combinations of the two over a range of stimulus amplitudes. For steps of target velocity, the image motion model was able to reproduce the very different closed-loop responses of the two monkeys we used. The model was also able to fit the closed-loop responses of the same two monkeys to sine wave perturbations over the frequency range of 2–10 Hz. Importantly, our nonlinear image motion model was able to reproduce responses to target velocity steps under conditions of delayed visual feedback, precisely the data that led Ringach (1995) to reject the image motion class of models.

Because the image motion model and the tachometer feedback model are formally very similar when target velocity is constant, the tachometer feedback model was able to reproduce the step responses of both monkeys. However, for accelerating targets, the tachometer feedback model performed poorly. It was unable to capture the differing degrees of saturation seen in open-loop pursuit responses to brief pulses and sinusoidal perturbations. Furthermore, when using reasonable values for the visual delay, the tachometer feedback model produced closed-loop responses to sinusoidal perturbations that were too small and showed too much phase lag at all but the lowest frequencies. These failures were in spite of both repeated optimizations (see METHODS) and the large number of free parameters available to the model. The shortcomings of the tachometer feedback model are understandable given its architecture. Because the model lacks sensitivity to image acceleration, it produces responses to accelerating targets that are smaller and more phase lagged than those of pursuit, and that show less saturation with increasing target acceleration.

We do not think that the shortcomings of the tachometer feedback model can be repaired by elaborating the details of the motor feedback (for example by adding further derivatives or more complicated filters). The motor feedback was included by Ringach (1995) so that the tachometer feedback model could emulate the image motion model when target acceleration was small or absent (e.g., for steps to a constant target velocity). The latency of the motor feedback is thus necessarily of the same order as the visuo-motor delay. However, the tachometer feedback model's failings are evident even during the open-loop period, before the proposed motor feedback could have an effect. Thus elaborating the motor feedback signal would not relieve the model's failings. We also do not think that elaborating the image velocity pathways of the tachometer feedback model would resolve its failings. For example, one might consider adding a second feed-forward image velocity signal to the tachometer feedback model, with a different filter or nonlinearity. However, if the response gain of this pathway were high enough to produce accurate responses to high-frequency sine waves, then responses to steps, pulses, and low-frequency sine waves would be overly large. Using multiple band-pass filters might achieve the desired amplitude responses for both high- and low-frequency stimuli. The phase would still lag, however, unless the visual delay were shortened considerably, which would then result in step and pulse responses that were too early. We do not see a way around the necessity for a visual signal, such as image acceleration, that creates phase lead without decreasing absolute latency. We therefore conclude that the pursuit system uses image acceleration information in guiding eye movements. The strength of this conclusion is, of course, tempered by the possibility that an as yet unexplored model might be able to account for the observed responses without using image acceleration information.

Although none of our experiments provides evidence for the use of eye acceleration–based motor feedback, none of our experiments or simulations rules out the possibility of such a signal. They show simply that such a motor signal cannot substitute for an image acceleration signal. In general, we interpret our results as evidence against all current pursuit models that do not use image acceleration information, or that assume the spontaneous oscillations are internally driven (e.g. Dicke and Thier 1999; Pola and Wyatt 2001). In particular, the original target velocity model of Robinson et al. (1986) lacks such a signal and is expected to exhibit failings similar to those of the tachometer-feedback model when presented with accelerating targets. In fact, the model of Robinson et al. (1986) has already been shown to produce overly phase-lagged responses for one frequency of sine wave perturbation (Goldreich et al. 1992).

Interpretation of model parameters

In the APPENDIX, we report the parameters and nonlinearities that allowed the image motion model to reproduce the pursuit responses. These features of the model are meant to describe aspects of the behavioral response and may not have distinct physiological correlates. For example, the delay in the image velocity pathway reflects the cumulative effects of delays in the retina, the visual pathways of the brain, and brain-stem motoneurons. The nonlinearity in the same pathway is meant to capture the behavioral response to image velocity and is indeed a reasonable approximation to the measured response function (Lisberger and Westbrook 1985). The "plant" filter is meant to incorporate both the mechanical properties of the plant and the properties of neural circuits that compensate for those mechanical properties (Skavenski and Robinson 1973). Thus, although the filtering properties of pursuit can be reasonably approximated with simple single-exponential filters, the underlying physiology is considerably more complex. In general, we wish to stress that our model is a model of behavior. While it has implications for the neural signals guiding pursuit, it is not a model of those neural signals. The goal of the model is to test the hypothesis that pursuit responses can be accounted for by assuming that eye acceleration is driven by a combination of signals related to image velocity and image acceleration.

Possible sources of visual information about image acceleration

Krauzlis and Lisberger (1991) demonstrated that the discharge of Purkinje cells in the floccular complex of the cerebellum could be accounted for as the sum of signals related to eye velocity and the three visual signals used by the image motion model: image velocity, motion onset transient, and image acceleration. The apparent use of an image acceleration signal by the pursuit system, and the presence of this signal in the cerebellum, raise the question of how image acceleration could be extracted from the discharge of motion-sensitive visual neurons. Motion-sensitive neurons in cortical area MT of rhesus monkeys are known to drive pursuit (Dursteler and Wurtz 1988; Groh et al. 1997; Komatsu and Wurtz 1989; Newsome et al. 1985). MT neurons are tuned for image velocity, but many also respond to changes in image velocity: a large percentage of MT cells exhibit a transient increase in firing when stimulus speed is accelerated over 128 ms to the preferred speed velocity (Lisberger and Movshon 1999). While these transient responses could form the basis of an image *acceleration* signal for increases in image velocity, recordings in anesthetized monkeys indicate that transients provide little information about image *deceleration* (Lisberger and Movshon 1999). The image acceleration signal used by our model provides both positive image acceleration and image deceleration information. Image deceleration information is crucial in preventing overshoots of target velocity and is therefore more important to the performance of most pursuit tasks than is positive acceleration information. Thus it does not appear that a sufficient representation of image acceleration is *explicitly* coded by the firing of MT cells. However, that MT cells are tuned for image speed implies that an adequate image acceleration signal could be extracted from their firing, provided that the nervous system can approximate mathematical differentiation.

If the MT population code of image speed is converted to an explicit scalar code of image speed, an image acceleration signal could be extracted through a number of methods. The more appealing of these methods use the well-known method of delayed normalization. If v is the input to delayed normalization and a is the output, then

$$a(t) = \frac{v(t)}{v(t-\Delta t)} - 1 = \Delta t \cdot \frac{[v(t) - v(t-\Delta t)]/\Delta t}{v(t-\Delta t)} \approx \Delta t \cdot \frac{\mathrm{d}v(t)/\mathrm{d}t}{v(t)} + O(\Delta t^2) \approx \Delta t \cdot \frac{\mathrm{d} \log v(t)}{\mathrm{d}t}$$

Delayed normalization naturally produces an output that is approximately proportional to the derivative of the log of the input. This is entirely in agreement with our use of an image acceleration signal based on a saturated version of image velocity, and with the data in Figs. 4 and 5. Delayed normalization could be produced by the nervous system via feedforward or feedback circuits using shunting inhibition (e.g., Heeger 1992), or via synaptic properties such as synaptic depression (Abbott et al. 1997; Chance et al. 1998; Markram and Tsodyks 1996). Also, although our model represents image velocity and acceleration information using separate pathways, signals related to image velocity and image acceleration need not be carried by different subsets of neurons. The signals may be separable functionally, yet conflated in the responses of single cells.

While humans can clearly discriminate an accelerating target from a decelerating one, it does not appear that humans directly perceive image acceleration. Whereas perception of velocity is not equivalent to the perception of changes in position, the perception of acceleration may be equivalent to the perception of changes in velocity, at least for near-threshold judgements (Werkhoven et al. 1992). This finding is not in conflict with our conclusion that pursuit is driven in part by image acceleration. We are not claiming that image acceleration information is coded explicitly within visual cortex or is provided to the perceptual system.

Role of extraretinal signals in extrastriate cortex

Neurons in the medial superior temporal sulcus (area MST) are known to carry extraretinal signals; they respond when the eye moves, even when there is no visual motion (Newsome et al. 1988; Sakata et al. 1983). Area MST is part of the pursuit pathway, and prior physiology and modeling studies have suggested that the extraretinal signals therein could provide a source of motor feedback (often termed "corollary discharge") regarding eye velocity (Dicke and Thier 1999; Newsome et al. 1988). Such motor feedback is exactly what is proposed by the target velocity model of Robinson, and could also form the basis of the eye acceleration signal used by the tachometer feedback model. However, this and previous modeling work (Goldreich et al. 1992; Krauzlis and Lisberger 1994b) demonstrates that the model of Robinson is incorrect and that motor feedback is unnecessary to explain pursuit behavior. Why then are there motor signals in MST? It should be noted that most models of pursuit, including the image motion model, implicitly use eye velocity feedback to accomplish the integration of eye acceleration to eye velocity. MST may be part of the pathway that accomplishes this integration. Alternately, the

extraretinal signals in MST may be involved in estimating target velocity for the purpose of engaging and disengaging pursuit (Huebner et al. 1992; Krauzlis and Miles 1996; Luebke and Robinson 1988; Mohrmann and Their 1995; Pola and Wyatt 2001; Robinson et al. 1986; Scheuerer et al. 1998). We conclude that, although their true role is still a mystery, the extraretinal signals in MST are probably not providing motor feedback of the type proposed by the models of Robinson et al. (1986) or Ringach (1995).

Implications for the control of motor output

One of the major control problems faced by the pursuit system is overcoming the negative impacts of feedback delays. The target velocity model of Robinson et al. (1986), the tachometer model of Ringach (1995), and the image motion model of Krauzlis and Lisberger (1989, 1994b) adopt three different strategies to overcome delays. The target velocity model negates the feedback, sacrificing the advantages of a negative feedback system to eliminate the disadvantages. The image motion model drives eye acceleration using a combination of image velocity and image acceleration, essentially using the outdated visual inputs to make an estimate of the current image velocity. The tachometer feedback model uses a similar strategy but employs the first derivative of the system's output, rather than of its input. Each of these models has fundamentally different implications for the basic organization of the neural circuits that generate pursuit eye movements, and each represents a strategy that could be applied to a variety of other motor behaviors. Many motor systems other than pursuit use visually derived error signals (e.g., reaching movements) and suffer from feedback delays as long or longer than that of pursuit. To overcome feedback instabilities, these systems may also use one or more derivatives of the error signal. The presence of such signals could be evaluated empirically. As in pursuit, the frequency of visually driven spontaneous oscillations would be diagnostic of the presence of higher derivatives, as would the response to visually introduced perturbations.

APPENDIX

We report the parameters and nonlinearities that allowed the image motion model to reproduce the data in Figs. 10*A*, 11, 12, and 13. Table A1 shows four sets of values, one for each figure, for the pure delays and filter time constants. There was some variation in the parameters across the four simulations, which was necessary to account for the different responses of different monkeys, and even of the same monkey on different days. For example, the visual delays used to fit the data of *monkey Na* shown in Fig. 10*A* were slightly shorter than those used to fit data from the same monkey shown in Fig. 12. This is expected because the data in Fig. 10*A* were collected after the data in Fig. 12, and intervening training on other pursuit tasks had in fact reduced the monkey's pursuit latency. The greatest variability in parameters was found in the filter time constants. In part this was due to a tradeoff between the latency provided by the pure delay and that provided by the filter. But with the exception of the "plant" filter, the time constants of the filters appeared under-constrained by the data sets we used, and good fits to the same data could often be obtained using rather different filter time constants (data not shown).

The four rows of Fig. A1 show the four sets of nonlinearities used to fit the image motion model to the data from Figs. 10*A*, 11, 12, and 13. Each column shows the nonlinearity for a particular gain element. The *first column* shows the image velocity pathway nonlinearity, which was constructed from three linear elements, joined at −4 and +4°/s. The image velocity nonlinearities used by the four fits were similar, each showing a small to moderate decrease in gain with increasing image velocity. The *second column* shows the motion onset pathway nonlinearity. As described previously, this pathway was not used in fitting the responses to target velocity perturbations imposed during ongoing pursuit and therefore is not shown for the fits to the data in Figs. 10*A*. The motion onset pathway was available to the model only when fitting the responses to 15°/s steps of target velocity in Figs. 11–13. However, for the data of *monkey Na* in Fig. 12, the pathway was not used by the optimization algorithm (i.e., its gain was zero) and therefore is not shown in Fig. A1. We implemented the motion onset pathway using an equation that saturated quickly to a horizontal asymptote with an exponential relaxation. This description provides continuity with the model of Krauzlis and Lisberger (1994b), and with behavioral analyses of the nonlinearities present at pursuit initiation (e.g., Lisberger and Westbrook 1985). Note, however, that because this pathway was used only when the models responded to the initial step of target motion (the pathway was not used for responses to perturbations during ongoing pursuit), and because these steps were always 15°/s in amplitude, only the value of the nonlinearity at 15°/s was ever used, and the shape of the nonlinearity was not constrained by our experiments. We acknowledge that the behaviorally observed motion onset transient probably is not mediated by a separate visual pathway and instead represents part of the response to image acceleration. We nonetheless included it as a separate pathway, as an aid to the tachometer feedback model, for the reasons previously discussed.

The *third column* of Fig. A1 shows the saturation of image velocity prior to the extraction of image acceleration within the image acceleration pathway. This nonlinearity was parameterized separately for positive and negative values using an equation that allows for nearly linear behavior, or for bounded or unbounded saturation

$$f(v) = g_1\left(\frac{2}{1 + e^{-sv}} - 1\right) + g_2 \log\left(1 + g_3 v\right)$$

where v is velocity, and g_1, g_2, g_3, and s are free parameters. In all cases, the nonlinearity chosen by the optimization algorithm showed considerable saturation. There was a tradeoff between this nonlinear-

TABLE A1. *Model parameters*

	Delay			Filter Time Constant				
	Velocity	Acceleration	Motion onset	Velocity	Acceleration	Motion onset	Plant	Dv/dt
Fig. 10*A*	62	65		25	21		21	12
Fig. 11	62	60	54	43	11	4	18	1
Fig. 12	72	77		55	4		15	4
Fig. 13	63	75	65	68	10	37	15	1

Values are expressed in ms. Values of the visual delays and filter time constants used by the image motion model to produce the fits shown in Figs. 10–13. The 3 columns on the left show the delays for the 3 visual pathways used by the model, as shown in Fig. 9*A*. The 5 columns on the right show the values of the time constants for the 3 filters applied to the outputs of the 3 visual pathways, the plant filter, and the filter associated with differentiation in the image acceleration pathway.

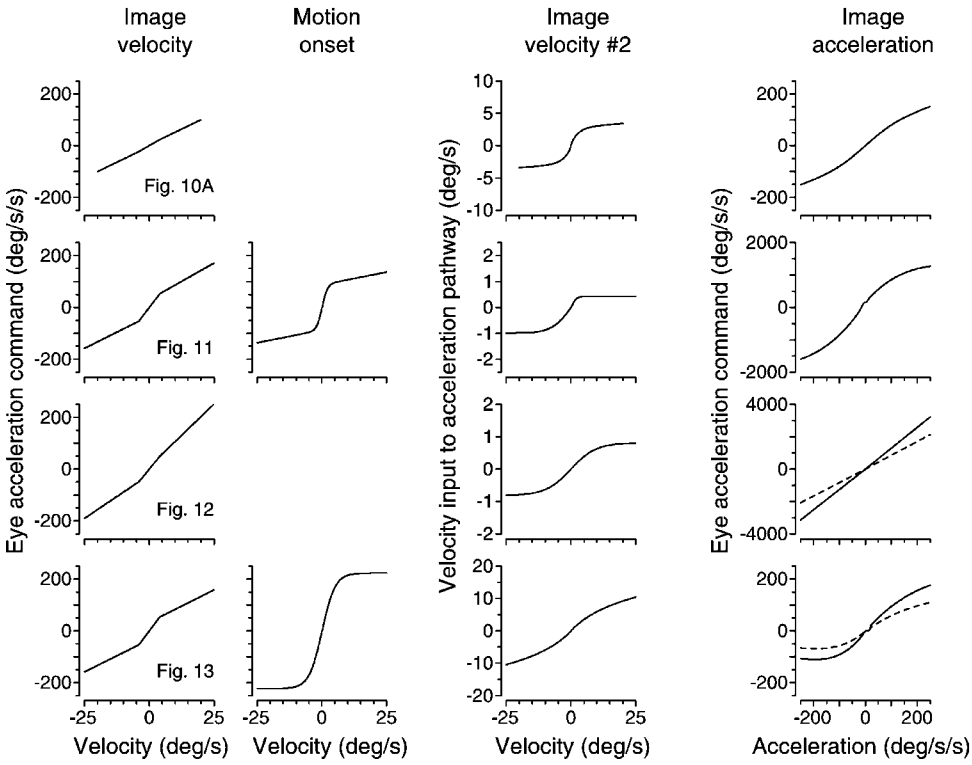

FIG. A1. Nonlinearities used by the image motion model to fit the data in Figs. 10–13. Each row represents a set of nonlinearities from a single optimization, used to fit the data indicated by the label at the *left*. The labels at the *top* of each column indicate where in the model the nonlinearities in that column were used. The "Image velocity" and "Motion onset" columns correspond to the nonlinear gain elements in the top and middle pathways of Fig. 9*A*. The "Image velocity #2" column corresponds to the saturation of image velocity prior to differentiation in the bottom pathway of Fig. 9*A*. The "Image acceleration" column corresponds to the 2nd nonlinearity in this pathway, situated after differentiation. The *x*-axis of each plot indicates the input to the nonlinear gain element, and the *y*-axis shows the output. The dashed curves in the *bottom 2 plots* for the image acceleration nonlinearity show how the gain of that pathway was reduced to provide fits to the data in Figs. 12*B* and 13*B*.

ity, acting on image velocity, and the subsequent nonlinearity acting on image acceleration (*4th column*). If the former was of low gain and/or high saturation, the latter was necessarily of higher gain, to maintain a similar overall gain of the pathway. Thus, even though the gains of these two elements differed dramatically among fits to the four data sets, the result was always an acceleration pathway with an overall gain that was either just above or just below the threshold for producing spontaneous oscillations. For the data in Fig. 11, good fits could be achieved using a symmetric saturation of image velocity (data not shown), but the best fit was achieved when this nonlinearity was somewhat asymmetric. As this monkey's responses to leftward pursuit were not reported in the original data of Goldreich et al. (1992), it is not known to what degree the asymmetric nonlinearity used by the model is related to a behavioral asymmetry. Behavioral asymmetries in pursuit are certainly common (e.g., Fig. 2 of Krauzlis and Lisberger 1994b).

The *fourth column* of Fig. A1 shows the second nonlinear gain element used in the image acceleration pathway. The nonlinearity was parameterized separately for positive and negative values using the equation

$$f(a) = g_1 a \cdot e^{-s_1 a} \cdot 1/(1 + g_2 e^{-s_2 a})$$

where a is the acceleration input, and g_1, g_2, s_1, and s_2 are free parameters. The first factor provides a linear gain, the second creates saturation, and the third creates a supra-linear gain near zero. These more elaborate features of the nonlinearity were helpful to a small degree in fitting the two models to the data in Figs. 11 and 13, but the only essential feature was some degree of saturation; good fits could be achieved without the supra-linear range near zero. The fits to the data in Fig. 10*A* were the last to be computed and used a simpler nonlinearity:

$$f(v) = g_1 a + g_2[2/(1 + e^{-sa}) - 1]$$

which contains only a linear and a saturating component. For the fits to the data in Figs. 12 and 13, two image acceleration curves are shown. The solid curve shows the gain used to provide fits to the 15°/s step responses. The dashed curve is identical in shape but scaled to illustrate the decrease in gain necessary to achieve fits to the sine wave perturbations of target motion.

We thank P. Churchland, A. Churchland, and the members of the Lisberger laboratory for helpful comments on an earlier draft of the manuscript. In particular we thank F. Crawford who created the java-based version of the model available on-line. S. G. Lisberger is an Investigator of the Howard Hughes Medical Institute.

M. M. Churchland was supported by a fellowship from the Department of Defense. Research was supported partly by National Eye Institute Grant EY-03878.

REFERENCES

ABBOTT LF, VARELA JA, SEN K, AND NELSON SB. Synaptic depression and cortical gain control. *Science* 275: 220–224, 1997.

CANNON SC AND ROBINSON DA. The final common integrator is in the prepositus and vestibular nuclei. In: *Adaptive Processes in Eye Movements and Vision*, edited by Keller EL and Zee DS. Oxford, UK: Pergamon, 1986.

CHANCE FS, NELSON SB, AND ABBOTT LF. Synaptic depression and the temporal response characteristics of V1 cells. *J Neurosci* 18: 4785–4799, 1998.

CHANDLER JP. STEPIT. University of Indiana Quantum Chemistry Program Exchange, 1965.

CHURCHLAND MM AND LISBERGER SG. Apparent motion produces multiple deficits in visually guided smooth pursuit eye movements of monkeys. *J Neurophysiol* 84: 216–235, 2000.

DAS VE, DISCENNA AO, FELTZ A, YANIGLOS S, AND LEIGH RJ. Tests of a linear model of visual-vestibular interaction using the technique of parameter estimation. *Biol Cybern* 79: 183–195, 1998.

DICKE PW AND THIER P. The role of cortical area MST in a model of combined smooth eye-head pursuit. *Biol Cybern* 80: 71–84, 1999.

DURSTELER MR AND WURTZ RH. Pursuit and optokinetic deficits following chemical lesions of cortical areas MT and MST. *J Neurophysiol* 60: 940–965, 1988.

FUCHS AF. Saccadic and smooth pursuit eye movements in the monkey. *J Physiol (Lond)* 191: 609–631, 1967.

GOLDREICH D, KRAUZLIS RJ, AND LISBERGER SG. Effect of changing feedback delay on spontaneous oscillations in smooth eye movements of monkeys. *J Neurophysiol* 67: 625–638, 1992.

GRASSE KL AND LISBERGER SG. Analysis of a naturally occurring asymmetry in vertical smooth pursuit eye movements in a monkey. *J Neurophysiol* 67: 164–179, 1992.

GROH JM, BORN RT, AND NEWSOME WT. How is a sensory map read out? Effects of microstimulation in visual area MT on saccades and smooth pursuit eye movements. *J Neurosci* 17: 4312–4333, 1997.

HEEGER DJ. Normalization of responses in cat striate cortex. *Vis Neurosci* 9: 181–198, 1992.

HUEBNER WP, LEIGH RJ, SEIDMAN SH, THOMAS CW, BILLIAN C, DISCENNA AO, AND DELL'OSSO LF. Experimental tests of a superposition hypothesis to explain the relationship between the vestibuloocular reflex and smooth pursuit during horizontal combined eye-head tracking in humans. *J Neurophysiol* 68: 1775–1792, 1992.

HUEBNER WP, SAIDEL GM, AND LEIGH RJ. Nonlinear parameter estimation applied to a model of smooth pursuit eye movements. *Biol Cybern* 62: 265–273, 1990.

JUDGE SJ, RICHMOND BJ, AND CHU FC. Implantation of magnetic search coils for measurement of eye position: an improved method. *Vision Res* 20: 535–538, 1980.

KELLER EL. Accomodative vergence in the alert monkey. *Vision Res* 13: 1565–1575, 1973.

KOMATSU H AND WURTZ RH. Modulation of pursuit eye movements by stimulation of cortical areas MT and MST. *J Neurophysiol* 62: 31–47, 1989.

KRAUZLIS RJ AND LISBERGER SG. A control systems model of smooth pursuit eye movements with realistic emergent properties. *Neural Comp* 1: 116–122, 1989.

KRAUZLIS RJ AND LISBERGER SG. Visual motion commands for pursuit eye movements in the cerebellum. *Science* 253: 568–571, 1991.

KRAUZLIS RJ AND LISBERGER SG. Temporal properties of visual motion signals for the initiation of smooth pursuit eye movements in monkeys. *J Neurophysiol* 72: 150–162, 1994a.

KRAUZLIS RJ AND LISBERGER SG. A model of visually-guided smooth pursuit eye movements based on behavioral observations. *J Comp Neurol* 1: 265–283, 1994b.

KRAUZLIS RJ AND MILES FA. Transitions between pursuit eye movements and fixation in the monkey: dependence on context. *J Neurophysiol* 76: 1622–1638, 1996.

LISBERGER SG AND MOVSHON JA. Visual motion analysis for pursuit eye movements in area MT of macaque monkeys. *J Neurosci* 19: 2224–2246, 1999.

LISBERGER SG AND WESTBROOK LE. Properties of visual inputs that initiate horizontal smooth pursuit eye movements in monkeys. *J Neurosci* 5: 1662–1673, 1985.

LUEBKE AE AND ROBINSON DA. Transition dynamics between pursuit and fixation suggest different systems. *Vision Res* 28: 941–946, 1988.

MARKRAM H AND TSODYKS M. Redistribution of synaptic efficacy between neocortical pyramidal neurons. *Nature* 382: 807–810, 1996.

MOHRMANN H AND THIER P. The influence of structured visual backgrounds on smooth-pursuit initiation, steady-state pursuit and smooth-pursuit termination. *Biol Cybern* 73: 83–93, 1995.

MORRIS EJ AND LISBERGER SG. Different responses to small visual errors during initiation and maintenance of smooth-pursuit eye movements in monkeys. *J Neurophysiol* 58: 1351–1369, 1987.

NEWSOME WT, WURTZ RH, DURSTELER MR, AND MIKAMI A. Deficits in visual motion processing following ibotenic acid lesions of the middle temporal visual area of the macaque monkey. *J Neurosci* 5: 825–840, 1985.

NEWSOME WT, WURTZ RH, AND KOMATSU H. Relation of cortical areas MT and MST to pursuit eye movements. II. Differentiation of retinal from extraretinal imputs. *J Neurophysiol* 60: 604–620, 1988.

POLA J AND WYATT HJ. The role of target position in smooth pursuit deceleration and termination. *Vision Res* 41: 655–669, 2001.

RASHBASS C. The relationship between saccadic and smooth tracking eye movements. *J Physiol (Lond)* 159: 326–338, 1961.

RINGACH DL. A tachometer feedback model of smooth pursuit eye movements. *Biol Cybern* 73: 561–568, 1995.

ROBINSON DA. The mechanics of human smooth pursuit eye movement. *J Physiol (Lond)* 180: 569–591, 1965.

ROBINSON DA, GORDON JL, AND GORDON SE. A model of the smooth pursuit eye movement system. *Biol Cybern* 55: 43–57, 1986.

SAKATA H, SHIBUTANI H, AND KAWANO K. Functional properties of visual tracking neurons in posterior parietal association cortex of the monkey. *J Neurophysiol* 49: 1364–1390, 1983.

SCHEUERER W, BUTTNER U, AND STRAUBE A. Prediction and a stationary, structured visual background influence the dynamics of the smooth-pursuit offset in humans. *Exp Brain Res* 123: 361–367, 1998.

SCHWARTZ JD AND LISBERGER SG. Initial tracking conditions modulate the gain of visuo-motor transmission for smooth pursuit eye movements in monkeys. *Vis Neurosci* 11: 411–424, 1994.

SKAVENSKI AA AND ROBINSON DA. Role of abducens neurons in vestibuloocular reflex. *J Neurophysiol* 36: 724–737, 1973.

TUSA RJ AND UNGERLEIDER LG. Fiber pathways of cortical areas mediating smooth pursuit eye movements in monkeys. *Ann Neurol* 23: 174–183, 1988.

UNGERLEIDER LG, DESIMONE R, GALKIN TW, AND MISHKIN M. Subcortical projections of area MT in the macaque. *J Comp Neurol* 223: 368–386, 1984.

WERKHOVEN P, SNIPPE HP, AND TOET A. Visual processing of optic acceleration. *Vision Res* 32: 2313–2329, 1992.

YOUNG LR, FORSTER JD, AND VAN HOUTTE N. A revised stochastic sampled data model for eye tracking movements. *Fourth Annual NASA-University Conference on Manual Control.* Ann Arbor, MI: University of Michigan, 1968.